Analyst

ROYAL SOCIETY OF CHEMISTRY

CRITICAL REVIEW

View Article Online
View Journal | View Issue

Cite this: *Analyst*, 2025, **150**, 1470

Recent advances in optical sensors for microcystin-LR: from recognition elements to signal transduction†

Heng Dai,‡[a] Jun Liu,‡[b] Shanlin Wang,[c] Bin Wang,[a] Tianhan Kai,[a] Pian Wu*[a] and Ping Ding *[a]

Microcystin-leucine-arginine (MC-LR), stands out as the most lethal and broadly occurring variant of microcystins, which are harmful substances generated by cyanobacteria during periods of excessive nutrient enrichment in water bodies. Even at low levels, MC-LR can cause acute or chronic hepatic injury, leading to inflammation and potentially promoting tumorigenesis, thereby imposing a significant burden on human health. Vigilant surveillance of MC-LR is vital for safeguarding both the well-being of the public and environmental security. Optical sensors are particularly advantageous for the detection of MC-LR, owing to their exceptional sensitivity and ease of use. This review presents a comprehensive overview of the current advancements and emerging trends in optical sensors for MC-LR detection, focusing on two primary aspects: recognition elements and optical signal transduction. Recognition elements, including enzymes, antibodies, molecular imprinted polymers (MIPs), and aptamers, are summarized along with their characteristics. The review also thoroughly discusses optical signal transduction and its performance, specifically addressing colorimetry, fluorescence, surface-enhanced Raman scattering (SERS), surface plasmon resonance (SPR), electrochemiluminescence (ECL) and other signal transduction methods. Additionally, the review provides a summary of the achievements and challenges of current optical sensors, as well as future application prospects for MC-LR optical sensors. This systematic review aims to facilitate the further development of optical sensors for detecting microcystins.

Received 26th December 2024,
Accepted 10th March 2025

DOI: 10.1039/d4an01576b

rsc.li/analyst

1. Introduction

The rapid increase of water eutrophication and global warming has led to frequent cyanobacterial blooms in many vital freshwater systems.[1] Within cyanobacterial blooms, microcystins (MCs), especially MC-LR, have emerged as a significant global concern due to their widespread occurrence and hepatotoxic effects on aquatic life and humans alike.[2,3] While aquatic creatures are predominantly at risk of encountering MC-LR, humans have a broader range of exposure pathways, including consumption, inhalation, dermal contact and direct intravenous exposure.[4] MC-LR has the ability to readily penetrate the body *via* the circulatory system, subsequently concentrating and inflicting harm on specific organs, such as the liver, reproductive glands, kidneys, heart, brain and so on.[5–10] Exposure to MC-LR in high doses can lead to conditions such as hepatomegaly, kidney failure, and severe gastrointestinal inflammation, and potentially be fatal.[5,11] Epidemiological and experimental perspectives suggest a correlation between MC-LR exposure and an increased risk of developing liver, prostate and colorectal cancers.[12,13] Considering the high toxicity of MC-LR, the World Health Organization has established a guideline that the maximum permissible concentration of MC-LR in potable water should not exceed 1 μg L^{-1}.[14]

Creating sophisticated and sensitive detection techniques for MC-LR is gaining greater significance. A variety of traditional analytical techniques have been recognized for detecting MC-LR, including the enzyme-linked immunosorbent assay (ELISA), protein phosphatase inhibition assay (PPIA), liquid chromatography-mass spectrometry (LC-MS) and high-performance liquid chromatography (HPLC).[15,16] ELISA is widely utilized for its specificity and sensitivity in determining MC-LR, despite that the detection procedures involved can be quite time-consuming and cumbersome. PPIA, one of the earliest detection assays for MCs, is straightforward but lacks the

[a]*Xiangya School of Public Health, Central South University, Changsha, Hunan, 410013, China. E-mail: wupian@csu.edu.cn, pingshui@csu.edu.cn*
[b]*University of South China, Hengyang, Hunan, 421001, China*
[c]*Guangzhou Customs District, Guangzhou, Guangdong, 510470, China*
†Electronic supplementary information (ESI) available. See DOI: https://doi.org/10.1039/d4an01576b
‡These authors contributed equally to this work.

ability to distinguish between different MC variants. LC-MS and HPLC are the predominant techniques used for the qualitative and quantitative analyses of various MC variants, however, they require sophisticated instruments and professional operators.

Compared to the conventional analytical methods, sensors demonstrate superiority in sensitivity, selectivity, and portability and have seen rapid advancements for detecting MC-LR.[17,18] Sensors are composed of two main parts: the recognition component and the signal transduction component. The recognition component engages with the target analyte, and the transducer converts this engagement into a signal that can be understood and processed.[19] Therefore, a systematic and comprehensive summary of the sensors for detecting MC-LR, focusing on recognition components as well as signal transduction, is of great significance. Existing review articles mainly focus on specific detection techniques or particular application scenarios. For instance, some reviews concentrate on DNA nanotechnology-based MC-LR detection, while others emphasize immunoassay methods.[16,20] There are also reviews that highlight the development of biosensors, electrochemical sensors or molecularly imprinted polymers (MIPs) for the recognition of MC-LR.[21–24] However, these reviews mostly cover only a single technique or application area without comprehensively summarizing advancements in optical signal transduction for detecting MC-LR. And no existing review systematically concludes the recognition elements for MC-LR. This review will cover the entire process from recognition elements to signal transduction, providing a comprehensive perspective on the latest advances in optical sensors for MC-LR detection.

In this overview, we have examined the majority of the studies and advancements in the field of optical sensor technology specifically aimed at detecting MC-LR. It primarily focuses on two key functional units of optical sensors: recognition elements and optical signal transduction (Fig. 1). Recognition elements, which encompass enzymes, biological antibodies, molecularly imprinted polymers (MIPs), and aptamers, along with their performance, are systematically introduced. The developments in optical signal transduction for MC-LR sensors are comprehensively summarized, specifically addressing colorimetry, fluorescence, surface enhanced Raman scattering (SERS), surface plasmon resonance (SPR), electrochemiluminescence (ECL) and other methods along with their underlying mechanisms. The review also highlights the significant applications of these sensors, focusing on linear ranges, detection limits (LOD), and practical applications. Furthermore, the current achievements, challenges and future trends in sensors for MC-LR are concluded. This systematic and comprehensive review aims to provide a crucial foundation for subsequent research on detecting MC-LR and even other cyanotoxins.

2. Recognition elements

Recognition elements, alternatively known as target receptors, which play a pivotal role in identifying and binding to specific

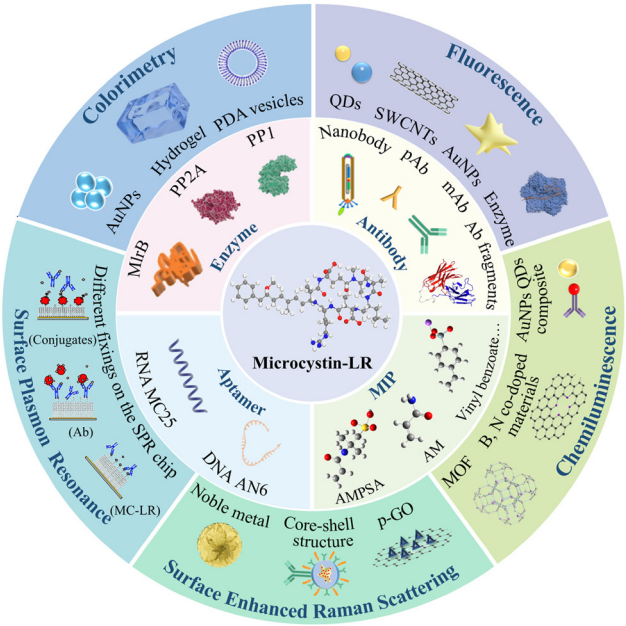

Fig. 1 The detection of MC-LR utilizing various recognition elements and multiple optical signal transduction methods.

analytes of interest, serve as crucial elements within sensors.[25] The selection of recognition elements is pivotal in ensuring the specificity and accuracy of the sensor to the target analytes. This section summarizes recent developments in recognition elements for detecting MC-LR, including enzymes, antibodies, MIPs, and aptamers.

2.1 Enzymes

MCs are capable of suppressing the function of protein phosphatases 2A (PP2A) and 1 (PP1). Consequently, PP2A and PP1 can be utilized as recognition elements in the construction of MC-LR sensors, as the inhibition of the protein serine/threonine phosphatases can be detected through various techniques. In 2011, Sassolas *et al.* investigated the inhibitory activity of MC-LR on various protein phosphatases (PPs), including one recombinant PP2A, two natural PP2As, and one molecular engineered PP1. Their findings revealed that the half-maximal inhibition concentration (IC_{50}) for the PP2As ranged from 0.21 μg L^{-1} to 1.55 μg L^{-1}, while the IC_{50} value for PP1 was found to be 0.56 μg L^{-1}.[26] In 2015, researchers led by Catanante developed an electrochemical biosensor for MC-LR utilizing recombinant PP1α, with the IC_{50} value for this recombinant PP1α being determined at 1.10 μg L^{-1}.[27] Despite the development of sensors utilizing PPs as recognition elements for MC-LR detection, these sensors exhibited a high rate of false positives due to the inhibition of protease activity by various other substances. Consequently, PPs have been increasingly supplanted by alternative recognition elements, for example antibodies and aptamers.

Recently, enzymes responsible for MCs degradation, expressed by bacteria, have been proposed as novel recognition

elements for detecting MC-LR. Li and colleagues created a sensor using the enzyme MlrB as a recognition receptor for MC-LR.[28] This sensor showed high sensitivity and specificity towards MC-LR, suggesting that these specific degradation enzymes could serve as effective recognition elements for MC-LR detection. However, extensive research is still necessary to fully establish the efficacy and practical application of these enzymes in sensor technologies.

2.2 Antibodies

Antibodies, characterized by their Y-shaped structure and ability to recognize specific molecules, are extensively utilized as recognition elements due to their exceptional specificity and binding affinity.[16] Polyclonal antibodies (pAbs) and monoclonal antibodies (mAbs) specific to MC-LR, as well as diverse antibody fragments, have been created and utilized for the identification and detection of MC-LR.

In 1996, Liu and colleagues selected nodularin as the idiotype antibodies (pAb1/r) to produce pAb2/m in mice. Subsequently, the purified pAb2 was then used as an immunogen to generated anti-anti-idiotype antibodies (pAb3/r) in rabbits. The resulting pAb3/r demonstrated high specificity to MC-LR, with an IC50 of 700 ng L^{-1}, but it also cross-reacted with various MC analogues. The IC_{50} values of pAb3/r for MC-YR, MC-RR, and nodularin were 19.2 μg L^{-1}, 24.4 μg L^{-1}, and 24.3 μg L^{-1}, respectively.[29] In 2000, Metcalf *et al.* developed a polyclonal IgG antibody against MC-LR by immunizing outbred Dutch rabbits. This antibody exhibited cross-reactivity with all microcystin and nodularin variants, including MC-LY, MC-LW, MC-LA and nodularin.[30] Subsequently, several other pAbs were produced by immunizing animals with MC-LR hapten.[31,32] For example, Xu *et al.* prepared a pAb with IC_{50} of 0.054 μg L^{-1} by immunizing New Zealand white rabbits with MC-LR -KLH.[33]

In comparison to pAbs, mAbs have garnered greater popularity in the development of MC-LR sensors. In 1995, Nagata *et al.* successfully produced six novel mAbs, designated as M1A6, M7D4, M8H5, M9D1, M1C2, and M1H4, which specifically recognized the Adda moiety of MC-LR. The affinity constants of these mAbs for MC-LR ranged from 1.5×10^{-7} to 3.1×10^{-10} L mol^{-1}, with M8H5 showing the highest affinity.[34] In a subsequent study, Zeck *et al.* generated a novel mAb (clone AD4G2) against the Adda moiety through the immunization of mice in 2001. The IC_{50} of AD4G2 for MC-LR was 330 ng L^{-1}.[35] To date, numerous mAbs with varying affinities to MC-LR have been produced, including MC4G7 (IC_{50} = 0.27 μg L^{-1}), C8C10 (IC_{50} = 1.12 μg L^{-1}), MC8C10 (IC_{50} = 1.50 μg L^{-1}), and MC10E7 (IC_{50} = 0.063 μg L^{-1}). These mAbs have been widely employed as recognition components in sensor technology.[36–43] Traditional antibodies (pAbs and mAbs) tend to be unstable.

In addition to mAbs and pAbs, antibody fragments have also been incorporated into the construction of MC-LR sensors. Murphy and colleagues generated a specific single-chain fragment variable (scFv) antibody fragment, designated 2G1. This 2G1 scFv exhibited an IC_{50} to MC-LR of 4.8 μg L^{-1}. However, the 2G1 scFv demonstrated comparable cross-reactivity to MC-YR, MC-LW, MC-LF, MC-LA, MC-RR and nodularin.[44] Xu *et al.* discovered 16 MC-LR-specific phage scFv antibodies from a library derived from a mouse immunized with MC-LR. Among them, the highest efficiency anti-MC-LR phage scFv, designated MscFv7, was efficiently produced in *E. coli* HB2151, demonstrating an IC_{50} of 471 ng L^{-1} against MC-LR. However, MscFv7 demonstrated notable cross-reactivity to MC-RR and MC-YR as well.[45] Hassanain *et al.* digested the MC-LR IgG antibody (110 kDa) to obtain Fab′ fragments (55 kDa) for the sensing of MC-LR. The reduced size of these Fab′ fragments provided advantages in surface coverage on nanoparticles, thereby enhancing the ability of the nanoparticles with specific functionalities to capture the target substance.[46] Additionally an A8 scFv was expressed and utilized to recognize MC-LR.[47]

It is noteworthy that nanobodies and recombinantly engineered antibodies have also emerged as advancements of MC-LR sensors. Researchers led by Pírez-Schirmer selected a highly sensitive nanobody (Nab A2.3) from a heavy-chain-only antibody (VHH) phage display library, with an IC_{50} value of 370 ng L^{-1}.[48] Xu and colleagues designed an innovative recombinant antibody (AV_{HH}–MV_H) *via* splicing anti-MC-LR mouse scFv (MscFv7) and anti-MC-LR alpaca nanobody (ANAb12) through chain shuffling technology, followed by random mutation *via* site-directed mutagenesis. This AV_{HH}–MV_H mutant demonstrated good stability and binding activity towards MC-LR (IC_{50} = 282 ng L^{-1}).[49]

Although a large number of antibodies have been quickly developed for the determination of MC-LR, studies have exposed weaknesses in their production: the use of mammalian expression systems makes the process of antibody production time-consuming and laborious. The performance variations among these pAbs, mAbs, antibody fragments, and recombinantly engineered AV_{HH}-MV_H in the recognition of MC-LR are summarized in Table 1.

2.3 Molecularly imprinted polymers (MIPs)

MIPs are tailored materials, which consist of highly cross-linked polymers with specific target molecular cavities. Biologically, MIPs are often referred to as "plastic antibodies" or "artificial antibodies" due to their selective recognition antibodies, which are analogous to specific antibodies.[22] MIPs are considered powerful recognition elements for developing precise detection techniques for various agents owing to their specific molecular recognition capabilities, high stability in terms of chemistry, mechanics, heat, ease of preparation and extended shelf life. In the molecular imprinting process, reactive monomers selectively bind to the reactive groups on the template molecule, leading to the construction of solid polymeric structures. After the template molecules have been extracted from the polymeric matrix, particular cavities remain, tailored for the re-association of the target molecules (Fig. S1†).[50] Therefore, the selection of functional monomers is crucial for synthesizing high-affinity MIPs for the target analyte.

In 2002, Chianella *et al.* screened five functional monomers for MC-LR employing computational techniques. An MIP, crafted through computational methods, was formulated using midazole-4-acrylic acid ethylester (UAEE) and 2-acrylamido-2-

Table 1 The performance of the produced antibodies against MC-LR

Type of antibody	Advantages	Disadvantages	Application	Name	IC_{50} for MC-LR ($\mu g\ L^{-1}$)	IC_{50} for MC variants ($\mu g\ L^{-1}$)	Ref.
pAb	High affinity, low cost	Low specificity	Preliminary screening	pAb3/r	0.7	MC-YR (19.2) MC-RR (24.4) Nodularin (24.3)	29
mAb	High specificity and sensitivity	Single epitope, sensitivity to environment	Precision quantitative detection	M8H5	0.125	MC-RR (0.118) MC-YR (0.295) MC-LA (0.479) Nodularin (0.623)	34
				AD4G2	0.33	MC-YR (0.33) MC-RR (0.46) MC-LY (0.43) MC-LW (0.43) MC-WR (0.35) MC-LF (0.70) MC-LA (0.42) Nodularin-R (0.16) Adda (0.43)	35
				MC4G7	0.27	MC-YR (0.22) MC-RR (0.28) MC-WR (0.29) MC-HtyR (0.6) MC-LY (>300) MC-LW (>300) MC-LF (>300) MC-LA (>300)	35
				C8C10	0.6	MC-YR (8.1) MC-RR (10.9) MC-LW (>1000) MC-LF (>1000) Nodularin (1500)	40
				MC8C10	1.50	MC-YR (11.0) MC-RR (17.8) MC-LF (>1000) MC-LW (>1000) Nodularin (2000)	39
				MC10E7	0.063	MC-YR (0.050) MC-RR (0.066) MC-WR (0.069) MC-HtyR (0.15) MC-LY (104) MC-LF (>1000) MC-LW (>1000) MC-LA (>1000) Nodularin (0.62) Adda (>1000)	43
Antibody fragment	Strong matrix penetration, high stability	Reduced affinity, complex expression	*In situ* analysis	scFv 2G1	4.8	MC-YR (8.06) MC-RR (7.99) MC-LF (7.11) MC-LW (10.08) MC-LA (6.42) Nodularin (9.28)	44
				MscFv7	0.471	MC-YR (0.548) MC-RR (0.506) MC-LW (4.86) MC-WR (856)	45
Nanobodies	Extremely small size, extreme stability	High development difficulty	Direct detection in complex samples	Nab A2.3	0.37	MC-YR (1.01) MC-RR (0.83) DM-LR (0.47) MC-LA (1.2) MC-LY (6.7) MC-LW (6.7) MC-WR (1.12) DM-RR (0.86) MC-LF (6.0)	48
Recombined antibody	Programmable design consistency	High technical threshold, lengthy development cycle	Ultra-sensitive detection, clinical detoxification therapy	AV_{HH}-MV_H	0.282	MC-YR (0.313) MC-RR (0.230) MC-WR (9.72) MC-LW (5.04) MC-LF (>2000) MC-LY (>2000)	49

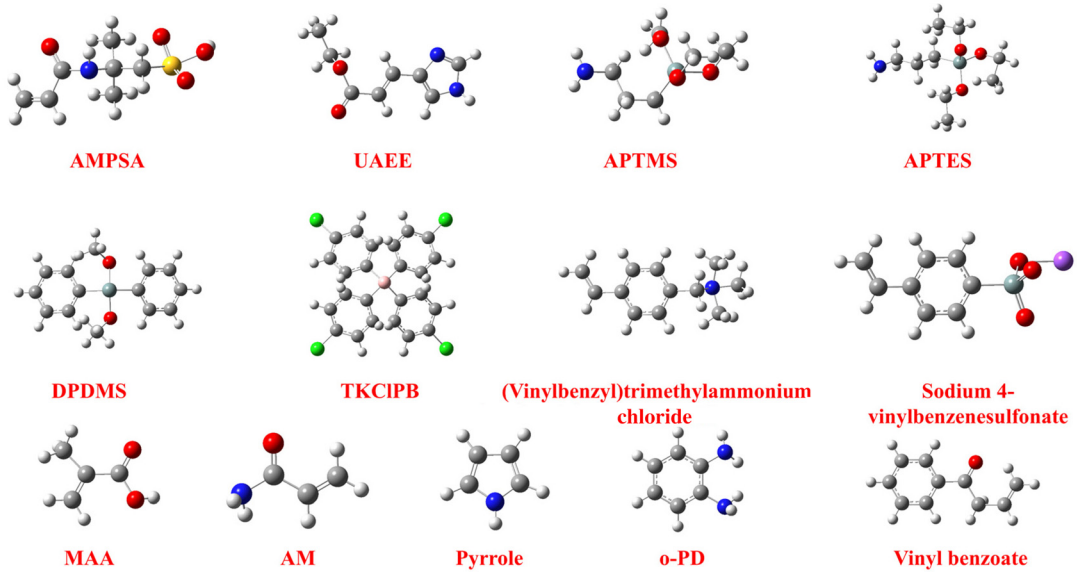

Fig. 2 The chemical structure of the organic functional monomers utilized while constructing MIPs for specific recognition of MC-LR.

methyl-1-propanesulfonic acid (AMPSA) as the reactive monomers. Compared to methacrylic acid (MAA)-MIP, the computational MIP exhibited an affinity for MC-LR (K_d = 0.3 ± 0.08 nM) that was more than threefold greater than that of MAA-MIP (K_d = 0.9 ± 0.1 nM). Importantly, the MIP showed minimal cross-reactivity with the analogues (MC-YR, MC-RR and nodularin), which is in stark contrast to the behavior of pAbs and even mAbs.[51] Zhao *et al.* employed density functional theory (DFT) calculations to determine the binding affinity of 4 monomers—methacrylic acid (MAA), acrylamide (AM), 2-aminothiophenol (*o*-ATP) and *p*-aminothiophenol (*p*-ATP)—towards L-arginine. They concluded that the combination of *p*-ATP and MAA was the most appropriate for the molecular imprinting of L-arginine.[52] Additionally, two sol–gel MIPs were synthesized. One was prepared using diphenyldimethoxysilane (DPDMS), (3-aminopropyl) trimethoxysilane (APTMS), and tetraethoxysilane (TEOS), and the other was made with (3-aminopropyl) triethoxysilane (APTES), TEOS, DPDMS and potassium tetrakis(4-chlorophenyl)borate (TKClPB). Both of these sol–gel MIPs demonstrated high specificity for MC-LR in the company of other species commonly found in environmental water samples.[53,54]

Recently, the integration of MIPs with inorganic nanomaterials to create MIP-based hybrids has garnered significant research interest. In these hybrids, MIPs serve as the recognition while inorganic nanomaterials are used for separation or signal output. For instance, Pan *et al.* engineered a graphene oxide-based ternary magnetic molecularly imprinted polymer hybrid (T-MMIP hybrid) for MC-LR. In this hybrid, GO-Fe_3O_4 served as the base within the in-position copolymerization involving a template molecule (MC-LR), a cross-linking agent (divinylbenzene, DVB) and functional monomer (AM). The resulting T-MMIP hybrid displayed selectivity not only for MC-LR but also for 8 variants (MC-WR, MC-LR, MC-YR, MC-LW, MC-LA, MC-LY, MC-LF and MC-RR).[55] Besides, Chen and colleagues employed pyrrole as the functional monomer in the fabrication of MC-LR imprinted polypyrrole (PPy) on a Cu_2O/ITO electrode *via* electropolymerization, which generated specific recognition sites that increased the electrode's selectivity for MC-LR.[56] Additionally, various other MIP-based hybrids have been fabricated, including MIP/CNTs,[57] MIP/Au NPs,[58] MIP@CQDs@SiO_2,[59] MIP/RGO/Ti–Fe–O NTs.[60] In these hybrids, functional monomers such as AMPSA, sodium 4-vinylbenzenesulfonate, (vinylbenzyl)trimethylammonium chloride, vinyl benzoate, APTES, and o-phenylenediamine (o-PD) were used to prepare MIPs on the surface of these nanomaterials. The organic functional monomers employed in the fabrication of MIPs targeting MC-LR are shown in Fig. 2.

Apart from organic MIPs, the incorporation of MC-LR recognition sites directly into the preparation process of inorganic photocatalytic MIPs has also been documented. Liu and colleagues synthesized a surface molecularly imprinted TiO_2@CNTs composite nanostructure (MI-TiO_2@CNTs) by directly integrating MC-LR as the template molecule into the precursor solution throughout the synthesis process of TiO_2 on CNTs. This method effectively embedded artificial recognition sites for MC-LR within the material. The MI-TiO_2@CNT-based sensor that was developed demonstrated exceptional sensitivity and selectivity in the detection of MC-LR.[61] MIPs offer distinct advantages in the recognition of MC-LR, such as high selectivity, cost-effectiveness, and stability. However, their complex preparation process, limited regeneration capacity and anti-interference capabilities can restrict their widespread application in certain scenarios.

2.4 Aptamers

Aptamers, referred to as chemical antibodies, are synthetically crafted short sequences of DNA/RNA oligonucleotides. These

molecules are chosen and amplified *in vitro* through a procedure referred to as systematic evolution of ligands by exponential enrichment (SELEX). Aptamers are characterized by their high stability, specificity, low cost, and ease of modification.[62]

In 2001, Nakamura and colleagues successfully developed the inaugural aptamer specifically designed to target MC-LR. However, this screened aptamer presented poor sensitivity towards MC-LR with a binding affinity (K_d) of 10^3 M^{-1}, and showed a higher specificity to MC-YR, limiting its applicability in developing sensors for MC-LR.[63] In 2004, Gu and Famulok identified four clone RNAs specific against MC-LR, among which MC25 clone RNA (5′-CCGGGGUAG GGA UGG GAG GUA UGG AGG GGU CCU UGU UUC C-3′) demonstrated relatively high affinity towards MC-LR with a K_d value of 4.6 μM.[64] In 2012, Ng and colleagues identified a range of DNA aptamers targeting MC-LA, MC-LR and MC-YR. Among them, AN6 (5′-GGC GCC AAA CAG GAC CAC CAT GAC AAT TAC CCA TAC CAC CTC ATT ATG CCC CAT CTC CGC-3′) exhibited the highest affinity towards MC-LR with a K_d of 50 ± 12 nM.[65] Since then, AN6 has been widely adopted in subsequent aptamer-based MC-LR sensors due to its favorable sensitivity and specificity. Aptamers offer several advantages in recognizing MC-LR, including high specificity, high sensitivity, and ease of functionalization. These characteristics make them particularly suitable for developing rapid and sensitive detection methods. However, challenges remain in their complex selection process, susceptibility to nuclease degradation, and non-specific adsorption, which need to be addressed.

3. Typical optical signal transduction

Signal transduction, the process that transfers the reaction information between the recognition elements and the targets into analytically useful signals, is another crucial component of sensors.[66] Effective signal transduction methods could significantly enhance the detection sensitivity of the target analytes. Among various transduction approaches, optical signal transduction has emerged as one of the most widely utilized in constructing sensors for detecting MC-LR due to its advantages such as straightforward operation, rapid response and robust stability.[17,67] Current optical sensors for MC-LR detection primarily focus on five signal output formats: colorimetry, fluorescence, surface-enhanced Raman scattering (SERS), surface plasmon resonance (SPR), and electrochemiluminescence (ECL). This section reviews recent advancements in sensors for MC-LR detection, with a particular emphasis on optical signal transduction.

3.1 Colorimetry

Due to its ease of use and simplicity, the colorimetric sensing method has become a robust analytical technique for detecting a wide array of analytes. A notable advantage of colorimetry is that signal change can be directly identified with the unaided eye. A key component in developing a colorimetric platform is converting the response behavior into a visual color change.[68]

Au nanomaterials are one of the most widely used materials in constructing optical sensors. In 2011, Zhu and colleagues reported a G-quadruplex DNAzyme-based immunosensor for detecting MC-LR. Within this research, G-quadruplex-hemin DNAzymes and secondary antibodies were coated on the Au NPs' surface as new labels (CatG4-AuNP conjugates). These CatG4-AuNPs conjugates could interact with the MC-LR antibodies through the secondary antibodies and could facilitate the H_2O_2-driven oxidation of ABTS to produce coloured products owing to the peroxidase activity of G-quadruplex-hemin DNAzymes (Fig. 3A). This immunosensor was specifically designed to detect MC-LR over a linear response range (100–10 000 ng L^{-1}), featuring a LOD at 50 ng L^{-1}.[69] Apart from serving as a supporting matrix, Au NPs possess the property of color-change due to the aggregation of particles. Li and colleagues engineered a sensor utilizing aptamers for the selective identification toward MC-LR, which was supported by the aggregation of AuNPs. Aptamers were anchored to the AuNPs' surface *via* coordination bonds between gold atoms and the nitrogen atoms, which in turn averted aggregation of AuNPs caused by salts. When MC-LR was introduced to the solution containing aptamer-protected Au NPs, the aptamers selectively bound to MC-LR, thereby losing their protective effect against salt-induced aggregation of the Au NPs. This interaction led to a color change of the Au NPs from red to violet–blue (Fig. 3B). This result suggested that the aptamer-based colorimetric sensor was effective for MC-LR detection, with a good linear response (0.5–7500 nM) and a LOD at 0.37 nM.[70] Furthermore, an Au NP dimers sensor formed by two DNA-Au NPs and an aptamer was used for colorimetric detection of MC-LR. Within the study, the aptamer underwent a conformational change to bind with MC-LR, leading to the dissociation of AuNP dimers and a shift in the solution's color from blue to red within a 5 minute timeframe (Fig. 3C). This Au NP dimer-based colorimetric sensor demonstrated a linear response range between 0.1 nM and 250 nM and a LOD of 0.05 nM.[71]

Polydiacetylene (PDA) vesicles also exhibit sensitive color changes due to conformational changes in the conjugated backbone of PDA, making them suitable for optical signal transduction. Xia and colleagues incorporated mAbs specific to MC-LR into PDA vesicles, thereby creating MC-LR-recognizing vesicles (PDA-anti-MC-LR). The specific immunological interaction between MC-LR and PDA-anti-MC-LR resulted in a color shift discernible by the unaided eye, attributable to the conformation change of the PDA.[72] In addition to direct color change caused by nanoparticle conformational change, indirect color reactions were utilized for signal transduction. For example, Tang and colleagues reported the employment of antibody-modified SiO_2-coated magnetic nanoparticles (Fe_3O_4@SiO_2) and aptamer-modified PDA/CuNPs to bind to distinct epitopes on MC-LR, creating sandwich-like complexes that were magnetically extracted. Following the reaction with bis(cyclohexanone)oxaldihydrazone (BCO), the copper in the

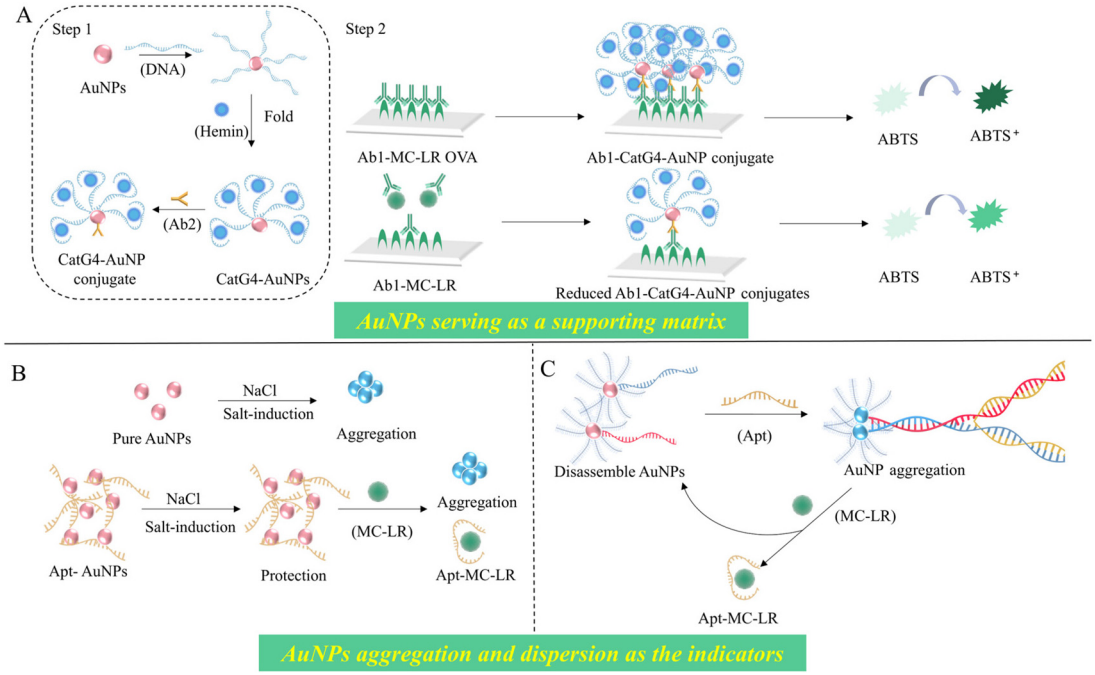

Fig. 3 (A) Design and process of G-quadruplex DNAzyme-based immunosensor for detecting MC-LR.[69] (B) Schematic illustration of the AuNP and aptamer-based colorimetric sensor and the associated analytical process for detecting MC-LR.[70] (C) Schematic illustration depicting the assembly and breakdown of AuNP dimers.[71]

extracted PDA/CuNPs was oxidized to Cu^{2+} ions, which led to a detectable absorption at 600 nm. It was discovered that the absorbance intensity demonstrated a linear correlation with MC-LR concentrations between 50 pM and 25 nM, featuring a LOD of 50 pM.[73]

Recently, the application of hydrogels in sensors has attracted great attention. Abnous *et al.* described a colorimetric sensor with graphene oxide (GO) incorporated within a hydrogel framework. The aggregation of GO sheets was induced by the interaction of complementary MC-LR aptamers and adenosine strands, with methylene blue (MB) sandwiched between the GO layers. Upon the introduction of MC-LR, the formation of the GO hydrogel structure was impeded due to the absence of complementary strands, causing the solution to turn blue that could be measured spectroscopically (Fig. 4A). This assay showed a LOD as low as 219 pM.[74] Additionally, in our previous study, we described a DNA hydrogel encapsulating Cu/Au/Pt trimetallic nanoparticles (Cu/Au/Pt TNs) for colorimetric sensing of MC-LR. Capitalizing on the heightened peroxidase-mimicking activity of the nanozymes, the developed colorimetric biosensor was able to sensitively quantify MC-LR within 4.0 ng L^{-1}–10 μg L^{-1}, with a LOD of 3.0 ng L^{-1} (Fig. 4B).[75]

Colorimetric signal transduction determination of MC-LR offers several advantages, such as ease of operation, low cost and rapid response, making it suitable for on-site rapid screening and preliminary detection. However, its application in high-precision and complex environments is limited by lower sensitivity, restricted quantitative performance, and susceptibility to interference. Therefore, colorimetric signal transduction usually needs to be combined with signal amplification strategies to enhance detection sensitivity.

3.2 Fluorescence

Fluorescence, recognized for its simplicity and high sensitivity, is one of the most commonly used signal output modalities in sensing platforms, ranging from biomedical diagnosis to environmental monitoring.[76] To date, numerous donor and acceptor fluorophores have been utilized in developing fluorescence sensors for MC-LR detection, encompassing quantum dots (QDs), fluorescent dyes, carbon-based materials, and gold nanomaterials, among others.[77]

QDs are potent materials for emitting fluorescence signals, boasting distinctive optical characteristics such as high quantum efficiency, narrow emission spectrum, photostability and extensive absorption. Feng *et al.* synthesized a CdSe/ZnS QD-hapten nanoprobe by linking carboxyl-functionalized CdSe/ZnS QDs to aminoethyl-MC-LR. The signal was facilitated by the fluorescence resonance energy transfer (FRET) occurring between the CdSe/ZnS QD-hapten nanoprobes and the Cy5.5-tagged antibodies. This sensor showed a good linear response (0.10–4.0 μg L^{-1}) and a LOD of 0.03 μg L^{-1}.[78] Similarly, in the study conducted by Lee *et al.*, they engineered a QDs-aptasensor employing the FRET approach, with magnetized QD525 (MB-QD525) functioning as the donor and the dimeric cyanine PoPo3 dye, which was integrated into the aptamer, serving as the acceptor. After the introduction of MC-LR, the aptamer recognized and bound to MC-LR, releasing PoPo3 molecules from the MB-QD525-aptamer–PoPo3

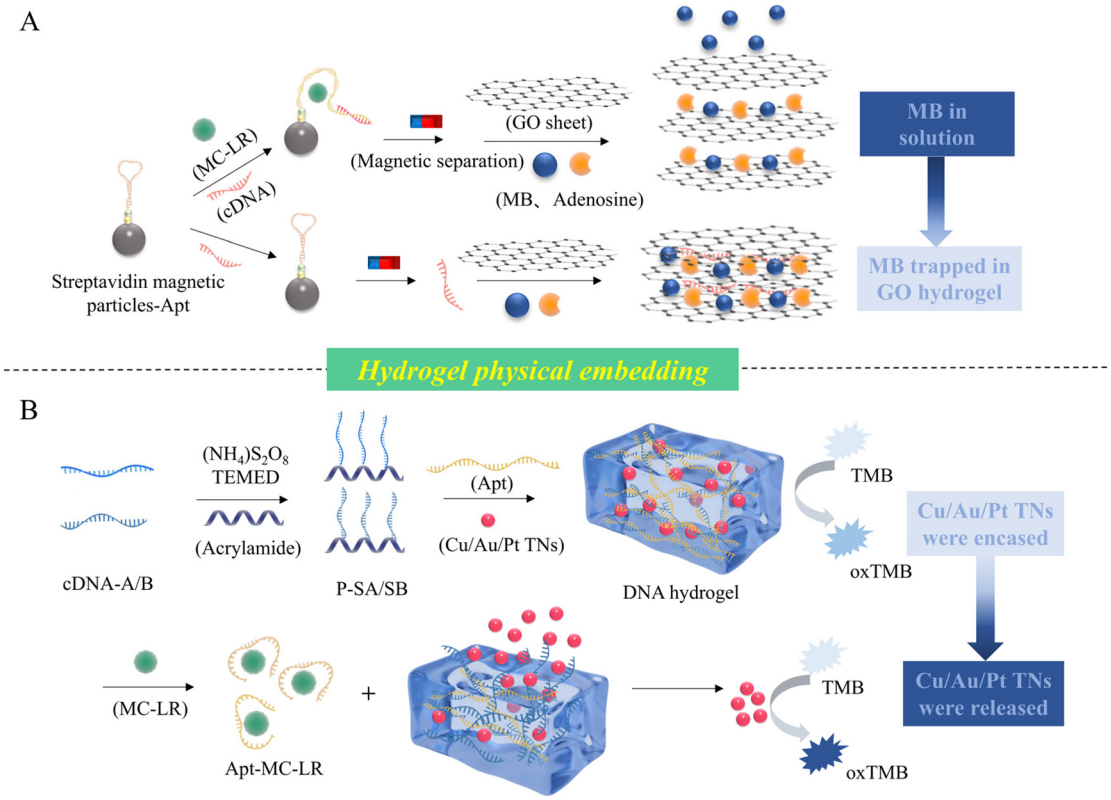

Fig. 4 Colorimetric determination of MC-LR. (A) Utilizing GO, a hairpin aptamer, and MB as an optical sensing element.[74] (B) Employing DNA hydrogel encapsulating Cu/Au/Pt TNs as a biosensor.[75]

complex, causing a decreased emission within the linear domain (0.1–100 μg L^{-1}) (Fig. 5A).[79] In addition to the FRET-based designs, the inner filter effect (IFE) between Au NPs and MoS_2 QDs was applied to design a fluorescence assay for detecting MC-LR by Cao and colleagues.[80] Fluorescence emission from MoS_2 QDs at 509 nm, upon excitation at 862/800 nm, was diminished owing to the presence of aptamer-modified Au NPs. Once MC-LR was added, the aptamer selectively bound to it. This binding caused the Au NPs to cluster in a saline environment, which in turn inhibited the fluorescence energy transfer. This process effectively restored the upconverted fluorescence of MoS_2 QDs (Fig. 5B). Capitalizing on the minimized background interference from the fluorescence upconversion of MoS_2 QDs, this aptasensor was used to identify MC-LR in actual water collected from the Gorges Reservoir area in China. It demonstrated a linear correlation from 50 pM to 40.19 nM with a LOD of 10 pM. Furthermore, Xu *et al.* used silane-doped carbon dots (Si-CDs) as fluorescence materials for ultrasensitive analysis of MC-LR. In their research, pAbs were labeled with horseradish peroxidase (HRP) for binding with MC-LR or coated MC-LR. Following the removal of unbound antibodies, the substrate solution consisting of H_2O_2 and ABTS was introduced. The HRP catalyzed oxidation of ABTS to its oxidized form (ox-ABTS) caused significant fluorescence quenching of the Si-CDs. (Fig. 5C). Variations in the fluorescence intensity of Si-CDs enable the quantitative detection of MC-LR in the range between 1 ng L^{-1} and 3.2 μg L^{-1} and provided a LOD of 0.6 ng L^{-1}.[33] Considering that MC-LR may influence the fluorescence of modified QDs, a novel "on–off–on" chemosensing approach was devised for detecting MC-LR using nitrogen and phosphorus co-doped carbon dots (N/P CDs). The fluorescence emission strength of the N/P CDs decreased in the presence of Fe^{3+} ions, which was attributed to the construction of Fe–O–P bonds between the Fe^{3+} ions and phosphorus-containing groups on the surface of the N/P CDs. However, upon adding MC-LR, the fluorescence intensity of N/P CDs could be recovered because of the rival coordination of the MC-LR cavity and Fe^{3+}. This strategy demonstrated a linear relationship (50–3000 ng L^{-1}), with a LOD of 17.1 ng L^{-1}.[81] Additionally, a fluorescence sensor based on molecularly imprinted polymer-coated carbon quantum dots (MIP@CQDs@SiO_2) was fabricated for detecting MC-LR, in which the fluorescence of CQDs was quenched after the adsorption of MC-LR through an electron transfer process.[59]

Carbon materials, for example single-walled carbon nanotubes (SWCNTs) and colloidal graphene (CG), have been exploited as transducers to translate recognition events into discernible fluorescence signals. Liu *et al.* utilized CG along with MC-LR-DNA conjugates to establish a rival fluorescence-based immunoassay for detecting MC-LR. The MC-LR-DNA probe rapidly adhered to the surface of CG through π–π stacking, which resulted in significant fluorescence quenching due

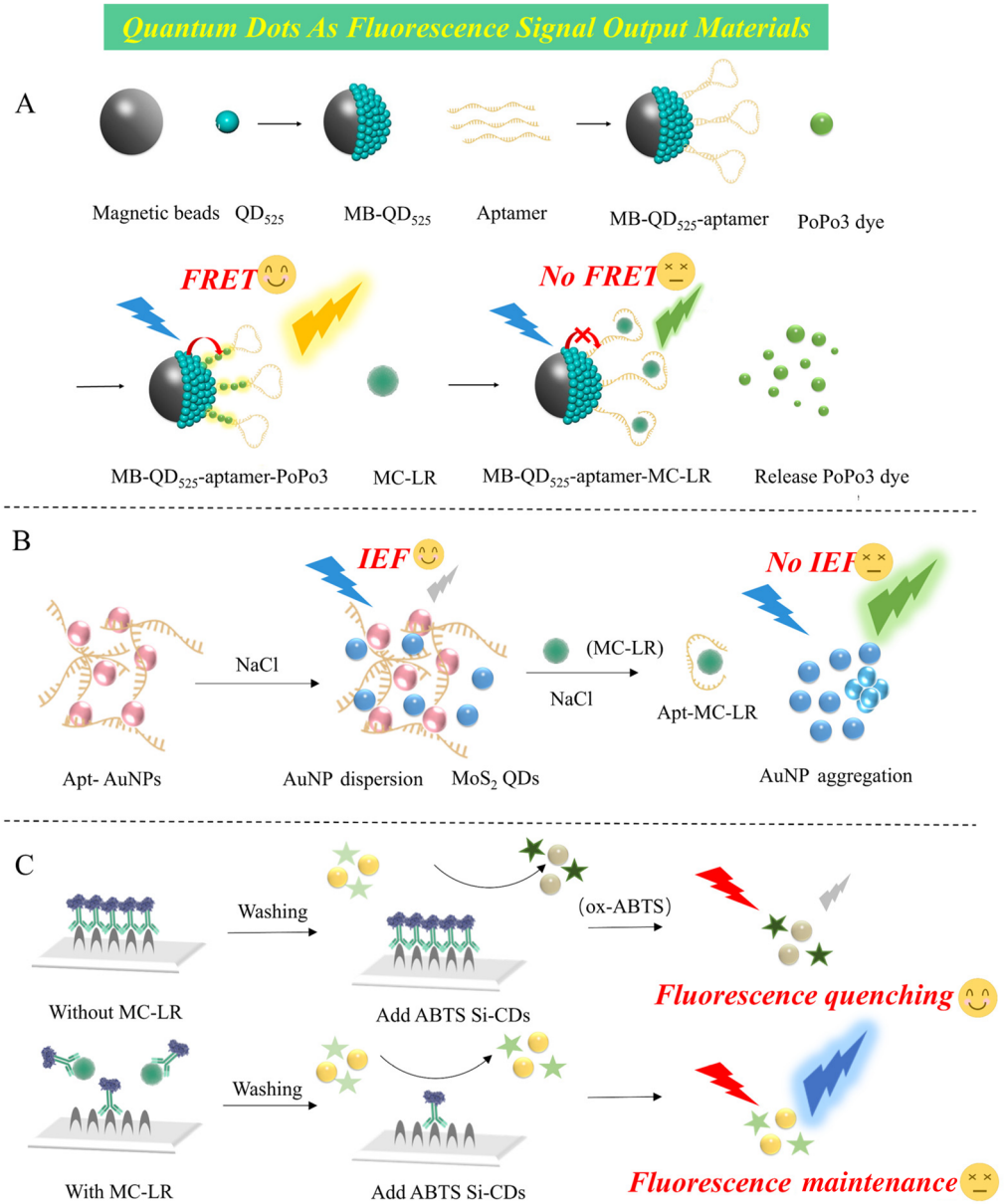

Fig. 5 (A) FRET based quantum QD525-aptasensor for detecting MC-LR.[79] (B) The MC-LR sensing mechanism involving MoS_2 QDs for upconversion luminescence and aptamer-conjugated Au NPs.[80] (C) The Si-CD-utilized FELISA technique for the quantitative analysis of MC-LR.[33]

to the excellent quenching performance of CG. On the other hand, the competitive interaction between MC-LR-DNA and anti-MC-LR antibodies disrupted the interaction between graphene and MC-LR-DNA, thereby causing the restoration of the fluorescence signal. The CG-based immunosensor enabled the quantitative detection of MC-LR, achieving a LOD of 140 ng L^{-1}.[82] In a separate investigation by Taghdisi *et al.*, SWNTs served as anchors for two distinct aptamers: one specific for MC-LR and another for a fluorescent marker (dapoxyl). Upon MC-LR being introduced, the aptamer designed to bind to the target detached from the SWNTs. This release enabled the aptamer specific to dapoxyl, which was also bound to the SWNTs, to interact with the dye, causing a decrease in fluorescence. The SWNT-based fluorescence sensor demonstrated a broad linear correlation with MC-LR concentrations (0.4–1200 nM) with a LOD of 138 pM.[83]

Au NPs, owing to their unique optical properties, are also a kind of the most popular nanomaterials in the construction of fluorescent sensors. Au NPs exhibit a surface-enhanced fluorescence (SEF) effect on the fluorophores positioned a few nanometers from the metal surface, while also possessing efficient fluorescence quenching capabilities. Li and colleagues engineered a SEF immunosensor that leveraged gold nano-crosses to amplify the fluorescence signal and employed Cy5 as the fluorescent marker molecule. The fluorescence of Cy5 could be enhanced by the Au nano-crosses without MC-LR

being present, since the Cy5-labeled goat anti-rabbit IgG was captured on the Au nano-cross-coated MC-LR-antibodies. Upon MC-LR being introduced, competitive interaction between the free and coated MC-LR for the MC-LR antibodies resulted in a decreased capture of Cy5-labeled goat anti-rabbit IgG on the Au nano-cross-MC-LR antibodies, leading to a decreased fluorescence intensity (Fig. 6A).[84] In a related study, Li *et al.* conjugated the Cy3 dye-labeled complementary ssDNA (Cy3-cDNA) to plasmonic gold nanostars (GNSs) to create Cy3-cDNA-GNS conjugates. The introduction of MC-LR-specific aptamers resulted in the formation of Cy3-cDNA/aptamer duplexes on the GNSs through the process of hybridization. The presence of MC-LR triggered the preferential binding of the MC-LR-specific aptamer to MC-LR, leading to the disassembly of the Cy3-cDNA/aptamer duplexes and causing fluorescence quenching as the Cy3 dye came into close proximity to the GNS surface (Fig. 6B). The fluorescence intensity under steady-state conditions varied directly with the MC-LR concentration spanning between 0.1 and 50 μg L^{-1}, exhibiting a LOD of 0.50 μg L^{-1}. Additionally, a surface-enhanced Raman spectroscopy (SERS) signal was also obtained with a LOD of 770 μg mL^{-1}.[85]

With the rapid advancements of biology, novel biological signal amplification strategies have been incorporated into the creation of a fluorescence sensor for detecting MC-LR. Xie *et al.* pioneered a nanofluidic system for the fluorescence identification of MC-LR. In their study, Au NPs adsorbed the FAM-labeled aptamers, quenching the fluorescence of FAM and protecting the aptamers from digestion by deoxyribonuclease I (DNase I) enzyme. The interaction of the aptamer with MC-LR resulted in the formation of an aptamer/MC-LR complex, subsequently releasing from the Au NP surface. Upon the introduction of the DNase I enzyme, it selectively digests the aptamers, which in turn releases MC-LR to serve as an additional target, enhancing the signal and leading to a strong fluorescence emission (Fig. 6C). This amplification approach, which incorporates the DNase I enzyme and AuNPs, demonstrated a broad linear response (0.25 nM–20 nM) and high sensitivity (LOD = 0.83 nM) toward MC-LR.[86] Recently, two novel CRISPR-based signal amplification strategies for fluorescence sensing of MC-LR were reported by Yan's and Wu's group, respectively.[87,88] In Yan's research, they developed an aptasensor platform, dubbed MC-LR-Casor, that leverages CRISPR-Cas12a for the on-site detection of MC-LR. Initially, the MC-LR-specific aptamer was annealed with a blocker DNA sequence and then attached to magnetic beads (MBs), causing the formation of the MB-aptasensor. Upon binding to MC-LR, the aptamers released the blocker DNA, thereby activating the CRISPR/Cas12a system. This activation led to the rapid cleavage of the fluorescence reporter, resulting in strong

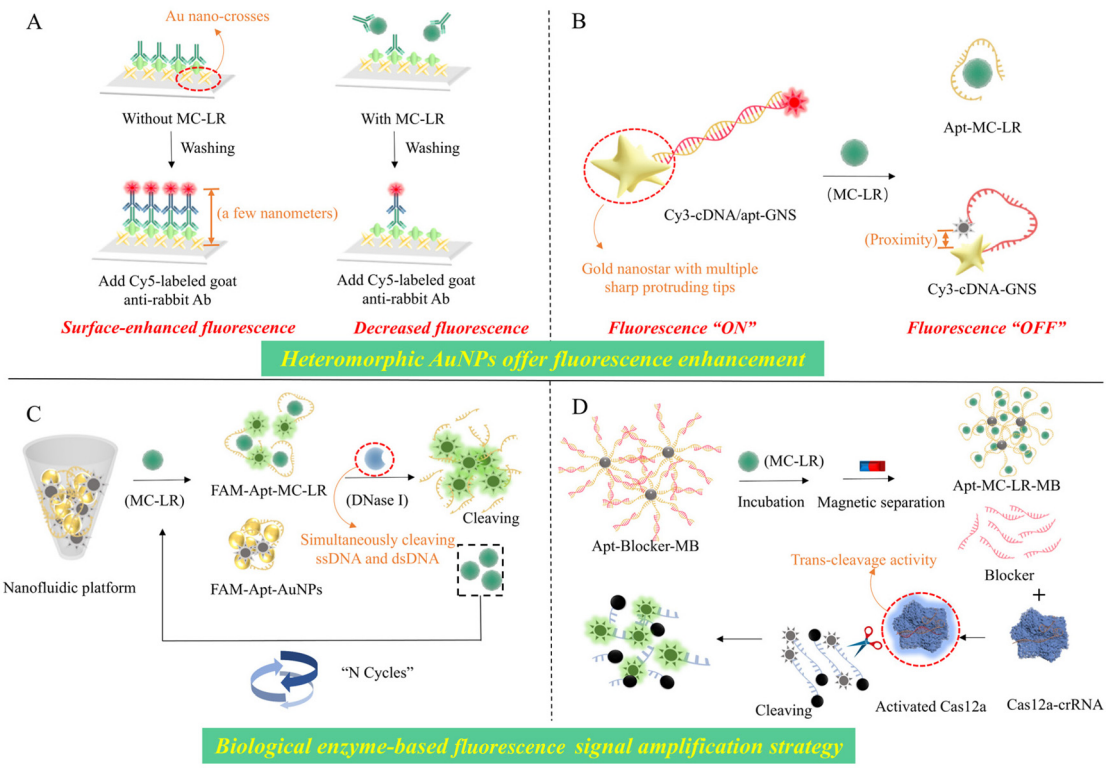

Fig. 6 (A) An SEF immunosensor incorporating Au nano-crosses for the identification of MC-LR.[84] (B) Diagram of the dual-function aptasensor utilizing both fluorescence and SERS for MC-LR detection, leveraging plasmonic GNSs.[85] (C) Schematic illustration of fluorescence detection of MC-LR relying on AuNP protected-aptamer and DNase I cleavage enzyme activity.[86] (D) Aptasensor employing CRISPR-Cas12a technology for the field detection of MC-LR.[87]

fluorescence (Fig. 6D). Leveraging the CRISPR/Cas12a amplification platform, the developed sensing system achieved a LOD of approximately 3 pg L^{-1}.[87] In our previous study, we developed an innovative and adaptable fluorescence sensor, termed the Cas14-pMOFs sensor, by fusing the CRISPR/Cas14a mechanism with two-dimensional sheets of porphyrin-based metal–organic frameworks (2D-pMOFs). In this setup, the FAM-labeled single-strand DNA (ssDNA-FAM) was adsorbed onto the Cu-TCPP(Fe) nanosheet to serve as the fluorescence indicator. The complementary DNA to the MC-LR aptamer (cDNA) was designed to act as an activator for the CRISPR/Cas14a system. When the MC-LR is exposed to its corresponding aptamer during incubation, the cDNA was released into the solution, triggering the trans-cleavage activity of Cas14a. This caused the cleavage of ssDNA-FAM into smaller DNA fragments and their subsequent desorption from the Cu-TCPP(Fe) nanosheets, which produced a fluorescence signal. The fluorescence sensor was capable of detecting MC-LR within the span between 0.05 ng mL^{-1} and 1000 ng mL^{-1}, with aLOD of 0.19 ng mL^{-1}.[88]

Fluorescence signal transduction offers several advantages in detecting MC-LR, such as high sensitivity, ease of operation and rapid response, making it suitable for on-site rapid screening and preliminary detection. However, the high cost of fluorescent dyes and their susceptibility to quenching by other factors also limit their application in actual samples.

3.3 Surface enhanced Raman scattering (SERS)

SERS is an analytical method that merges the molecular selectivity of Raman spectroscopy with the distinctive optical characteristics of plasmonic nanoparticles. In the SERS system, the electromagnetic field at the surface of nanostructured metallic particles is significantly enhanced due to the plasmonic effects, resulting in an amplification of the SERS signal intensity across multiple orders of magnitude.[89] This amplification enables highly sensitive detection, down to the single-molecule level. SERS offers several advantages, including label-free and nondestructive characterization, as well as a rapid response time, making it a powerful analytical tool for biomedical diagnostics and environmental monitoring.[90,91]

Great strides have been achieved in SERS-based detection systems for tracking MC-LR, primarily concentrating on creation and fabrication of SERS substrates. Noble metals such as Ag and Au are among the most popular materials for SERS substrates, offering enhancement factors up to the order of 10^{14}.[90] In 2015, Zhao *et al.* fabricated SERS-active Au nanoflower-Ag nanoparticles (Au NF-Ag NPs) core–satellite assemblies, using the Y-shaped aptamer hybrid chains to assemble the Au NFs and Ag NPs. The SERS-active assemblies exhibited a substantial enhancement of the local electromagnetic field. With the introduction of MC-LR, the assemblies disassembled, causing a reduction in the SERS signal intensity (Fig. 7A). A direct proportionality was found between the SERS signal intensity of the assemblies and the MC-LR concentrations, spanning between 10 pM to 10 nM, with the LOD reaching 8.6 pM.[92] Similarly, Wei *et al.* modified cDNA and 4-ATP onto Au NPs to prepare a SERS tag and constructed a hairpin aptamer modified magnetic sphere. When MC-LR is present, the hairpin aptamer would open, allowing the SERS tag to connect

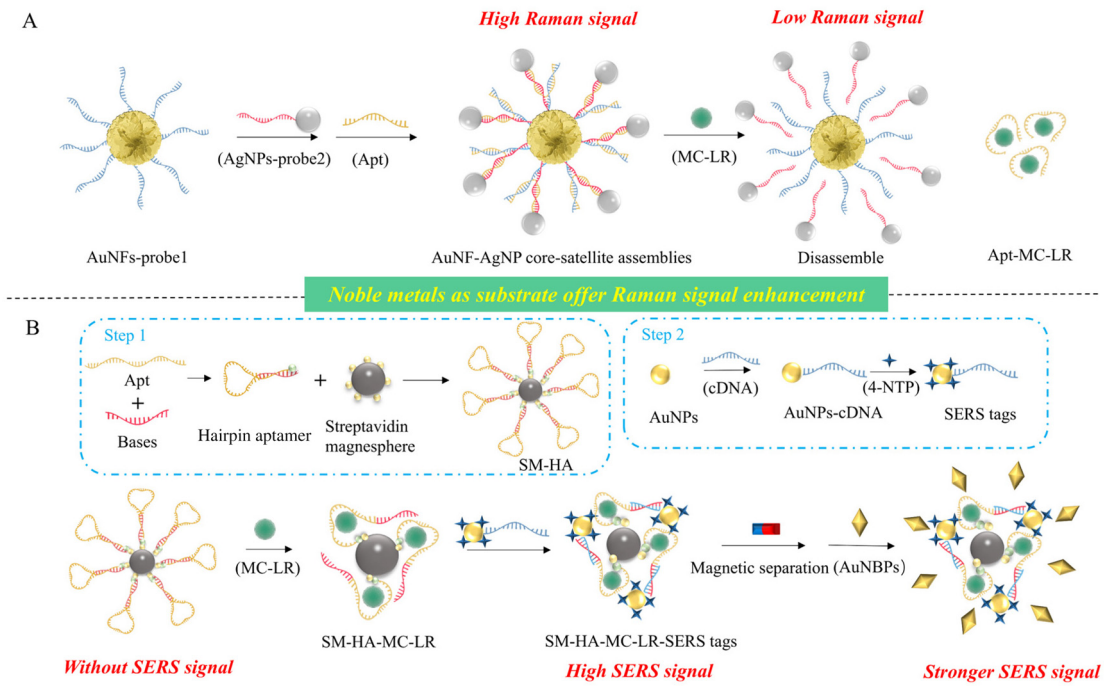

Fig. 7 (A) Schematic depiction of the synthesis process of SERS-responsive Au NF-Ag NP core–satellite configurations aimed at detecting MC-LR.[92] (B) Schematic illustration of the operational principle of the hairpin aptamer-based sensor for detecting MC-LR.[93]

to the hairpin aptamer through complementary bases (Fig. 7B). As a result, notable Raman signals were produced following magnetic separation, with MC-LR concentrations varying from 100 pg L^{-1} to 100 μg L^{-1}.[93]

To further enhance the local electromagnetic field, core–shell nanostructures with ultra-small gaps were fabricated as SERS probes. The Raman reporter could be situated in the interstice between the core and the shell, acting as internal standards, and shielded from external environmental perturbations by the shell. Zhao *et al.* successfully synthesized SERS-active Au@AgAu nanoparticles with a tunable gap that enhanced the SERS activity. These Au@gap@AgAu nanoparticles were combined with GO/Fe_3O_4 nanoparticles through π–π stacking interactions between the GO and the MC-LR aptamers. With MC-LR being present, the Au@gap@AgAu nanoparticles detached from the GO/Fe_3O_4 nanoparticles because of the aptamers' binding specificity, resulting in a reduced Raman intensity of the SERS tags (Fig. 8A). This SERS-based sensing method demonstrated improved reliability and reproducibility for detecting MC-LR, with a linear detection varying from 10 pM to 100 nM and a LOD of 9.82 pM.[94] Luo *et al.* developed a core–dual shell structured SERS tag consisting of layers of an Au core with a SERS label, a silver shell, and an outer gold shell (Au@label@Ag@Au NPs). The inner Ag shell layer enhanced the plasmonic enhancement and protected the SERS label from environmental interference, while the outer Au shell layer prevented the oxidation of Ag and improved biocompatibility. By attaching aptamers to the outer gold shell, the Au@label@Ag@Au nanoparticles were anchored onto asymmetric gold nanoflowers (AuNFs) that were spread on flat silicon substrates *via* DNA hybridization, creating core–satellite nanostructures on these substrates. Introducing MC-LR led to the dissociation of Au@label@Ag@Au NPs from the AuNFs, leading to a weaker SERS signal. Notably, this SERS aptasensor is capable of detecting MC-LR and MC-RR, either separately or together, by adopting two different SERS labels, 4-mercaptobenzonitrile (4-MBN) and 4-nitrothiophenol (4-NTP), each with specific aptamers.[95] Additionally, Li *et al.* constructed a SERS tag by coating silica onto the Raman molecule modified plasmonic gold nanostar (GNS) cores (GNS@Raman reporter@SiO_2). A SERS immunoassay was designed by immobilizing the mAb onto both GNS@Raman reporters@SiO_2 and the quartz chip. The stepwise introduction of MC-LR targets and SERS probes facilitated the formation of a sandwich-like complex, which was subsequently analyzed using SERS technology (Fig. 8B). This SERS sensor displayed a linear dynamic detection range from 10 ng L^{-1} to 100 μg L^{-1} and reached a LOD of 14 ng L^{-1}. Importantly, this SERS sensor demonstrated valuable applicability in continuously monitoring dynamic MC-LR production by a *Microcystis aeruginosa* culture.[96]

Graphene-derived plasmonic nanohybrids have likewise been utilized for the fabrication of SERS sensors. To achieve ultrasensitive detection of MC-LR, Ma *et al.* reported a real-time assembled SERS aptasensor based on hollow triangular

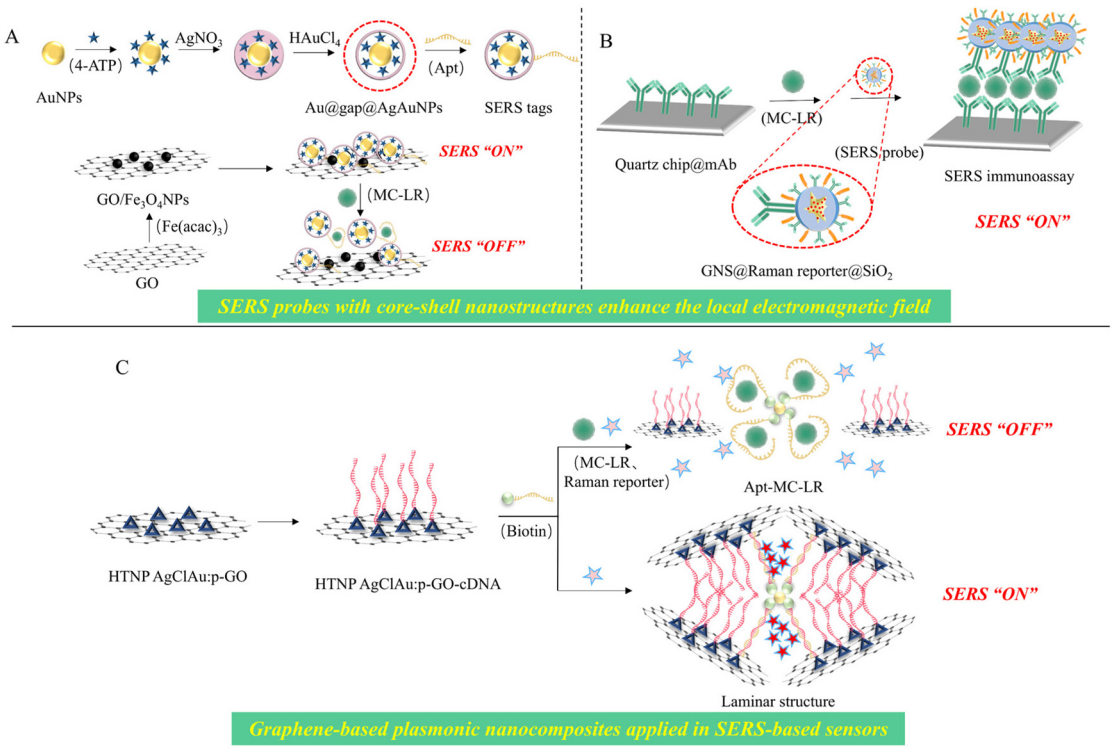

Fig. 8 (A) Schematic representation of constructing a Raman IS-aptasensor utilizing Au@gap@AgAu NPs-GO/Fe_3O_4 NP complexes for MC-LR detection.[94] (B) SERS-based immunodetection of hepatotoxic MC-LR.[96] (C) Schematic depiction of the rapid assembly of HTNP AgClAu : p-GO nanocomposites modulated by aptamers for sensing MC-LR.[97]

nanoplate AgClAu:plasmonic graphene oxide (HTNP AgClAu:p-GO) nanocomposites. In this system, the HTNP AgClAu:p-GO nanocomposites were assembled from networks to a laminar structure through DNA hybridization using a biotin–streptavidin interaction protocol, with Raman reporters simultaneously embedded into the laminar structures. The dynamic assembly procedure could be adjusted in real time with the ratiometric introduction of MC-LR, causing an alteration of the SERS signal (Fig. 8C). This real-time controllable aptasensing approach attained a broad linear response between 0.01 nM and 5 nM and n LOD of 6.3 pM.[97]

In addition to a single Raman signal output, dual-mode signal transduction has been employed in detecting MC-LR. Tian *et al.* proposed a dual sensing strategy that combines SERS and FET technologies, utilizing AuNPs/GO composites as the sensing material. This dual-mode biosensor allows for detecting MC-LR qualitatively *via* its Raman fingerprint spectrum, while quantitatively determining MC-LR through the graphene field effect transistor.[98]

SERS significantly amplifies Raman signals, thereby greatly enhancing detection sensitivity and even enabling single-molecule detection. This is highly advantageous for detecting low concentrations of MC-LR. Additionally, SERS can simultaneously detect multiple analytes, offering multiplexing capabilities that make it suitable for analyzing complex samples. However, the repeatability of SERS signals is influenced by the properties of the substrate materials. Commonly used metallic substrates like Ag and Au have trade-offs. Ag provides the best enhancement effect but is less stable, whereas Au is more stable but offers weaker enhancement and is more expensive. These factors limit the large-scale application of SERS in the detection of MC-LR.

3.4 Surface plasmon resonance (SPR)

SPR technology is an optical-based approach utilized to measure the refractive index of an ultrathin layer of material adsorbed on a metal surface. The SPR-based sensing strategy offers several advantages, including automation, real-time detection, reuse and reproducibility, making it an ideal candidate for signal output applications.[99,100]

Herranz *et al.* modified the SPR chip with a self-assembled monolayer (SAM) and then covalently attached MC-LR to the SAM for detecting MC-LR. This refined SPR biosensor achieved an IC_{50} value of 0.67 ± 0.09 μg L^{-1}, covered a dynamic range between 0.2 and 2.0 μg L^{-1}, and had a LOD of 73 ± 8 ng L^{-1} for MC-LR. Capable of conducting four simultaneous measurements within 60 minutes, each SPR chip could be utilized in a minimum of assay and regeneration cycles without substantial decrease in binding affinity. However, this SPR biosensor exhibited high cross-reactivities towards MC-RR (88%) and MC-YR (94%).[101] Devlin *et al.* covalently attached MC-LR to a CM5 chip and used it in a competitive assay with a 4-minute injection period using an in-house produced mAb to detect total MCs. This assay not only had the sensitivity to detect extracellular MC-LR at 0.5 ng mL^{-1} but also could quantify intracellular microcystin concentrations with a LOD of 50 pg mL^{-1}.[102] Tan *et al.* developed a SPR system that uses frequency-shifted light of different polarizations to stimulate laser heterodyne feedback interferometry (LHFI). This technique amplifies the reflectivity change caused by refractive index (RI) variations on a gold-coated SPR chip surface. The s-polarized light serves as a reference to compensate for noise, thereby enhancing RI resolution. Using antibodies as recognition elements, the system achieves ultralow detection limits for MC-LR (3.9 ng L^{-1}).[103] Practical and automated, the SPR/ESP/LRAUV system developed by William *et al.* integrates an SPR instrument with an environmental sample processor (ESP) and a long-range autonomous underwater vehicle (LRAUV) to detect and quantify particle-associated MCs (pMCs). This system complements existing cyanobacterial harmful algal blooms survey techniques and enhances predictive models for bloom and toxicity forecasts.[104]

SPR signal transduction offers several advantages, such as real-time monitoring and high sensitivity, making it particularly suitable for studying the interactions between MC-LR and recognition elements, as well as for detecting low concentrations of MC-LR. However, it also has drawbacks, such as expensive instrumentation and a high dependence on functionalization of the chip surface.

3.5 Electrochemiluminescence (ECL)

ECL refers to the light emitted from the excited state of the ECL luminophore, which is generated on the electrode surface *via* a high-energy electron transfer process that includes electrochemical reactions. The technique integrates the advantages of both electrochemical and spectroscopic techniques, offering high sensitivity, good specificity, a broad linear range, and cost-effectiveness.[105,106]

Graphene materials co-doped with boron (B) and nitrogen (N) have garnered significant interest for their remarkable luminescence characteristics, particularly in the development of ECL sensors. Wang's team has created a suite of ECL sensors for detecting MC-LR, leveraging B,N co-doped graphene. In their initial setup, the co-doped graphene hydrogels (BN-GHs) were utilized to enhance the steric interference between MC-LR and its corresponding aptamer. With the increasing concentration of MC-LR in the system, the ECL signals progressively diminished. This reduction occurred because the specific binding between MC-LR and its aptamer obstructed the approach of the coreactant TPrA to the Ru $(bpy)_3^{2+}$ on the electrode surface, leading to a lowered ECL emission. A direct correlation was observed between the decline in the ECL signal and the increasing concentrations of MC-LR, spanning from 100 fM to 1 nM, with a LOD of 30 fM.[107] To enhance the ECL response of B,N co-doped graphene, they designed a luminescent reagent by compositing ZnO QDs and B,N co-doped graphene (BNG/ZnO). By utilizing BNG/ZnO as the ECL luminophore and an aptamer for specific target identification, they developed a cathodic ECL aptasensor for detecting MC-LR. Within this setup, the ZnO quantum dots produce intense ECL emission through their interaction with $K_2S_2O_8$, and the incorporation of B and N into the gra-

phene matrix substantially boosts the ECL signal strength (Fig. 9A). This synergistic enhancement resulted in a low LOD of 30 fM and a broad detection range from 100 fM to 5 nM.[108] Moreover, in order to further improve sensor performance, SPR induction-enhanced ECL technology was introduced. The approach incorporated B and N co-doped graphene quantum dots (BN-GQDs) for luminescence and bismuth nanoparticles (Bi NPs) to generate SPR. Lacking MC-LR, BN-GQDs were linked to Bi NPs through the hybridization of the MC-LR aptamer and its complementary DNA, allowing the ECL emission of BN-GQDs to induce SPR in Bi NPs, which in turn strengthened the ECL response of BN-GQDs, resulting in a high and enhanced ECL signal. However, with MC-LR being introduced, BN-GQDs could not be linked to the Bi NPs, so that the ECL signal decreased (Fig. 9B). Compared to the BN-GHs and BNG/ZnO, this SPR enhanced ECL sensor was beneficial for broadening the detection range (0.01–5000 pM) and enhance the sensitivity (LOD = 0.003 pM).[109] In addition to B and N co-doping, the incorporation of P can also enhance the ECL efficiency of CDs and allows for fine-tuning of the ECL wavelength.[110]

Other materials, including Au NPs, CdS QDs, metal–organic frameworks (MOFs) and copper nanoclusters (CuNCs), have been used as ECL transducers.[112] In research conducted by Zhang *et al.*, a sandwich-type ECL immunosensor was crafted for detecting MC-LR, incorporating Au NPs and CdS QDs. The Au NPs were deposited on a glassy carbon electrode (GCE) to link with the primary antibody specific to MC-LR (Ab1) and to enhance electron transfer. Meanwhile, CdS QDs were prepared and tagged to the secondary antibody (Ab2), serving as the ECL luminescent labels. With MC-LR being introduced, a sandwich structure was formed, resulting in a strong ECL signal emission *via* the electron transfer interaction between the CdS QDs that accept electrons and the reduced forms of $S_2O_8^{2-}$ in a phosphate-buffered solution. (Fig. 9C) This ECL immunosensor possessed a linear response to MC-LR ranging from 10 ng L^{-1} to 50 μg L^{-1} with a LOD of 2.8 ng L^{-1}.[111] MOFs possess high porosity, large specific surface areas and tunable chemical properties, making them one of the most popular materials for ECL.[113] Li *et al.* established an ECL-resonance energy transfer (RET) system for MC-LR monitoring based on 3,4,9,10-perylenetetracarboxylic acid/the metal–organic frameworks NH_2-MIL-125(Ti) (PTCA/NH_2-MIL-125) and Au NPs. In this system, complementary DNA1 and DNA2 were bound to the surface of PTCA/NH2MIL-125 and AuNPs, separately. The specific MC-LR aptamer served as a linker to connect the DNA1-PTCA/NH_2MIL-125 and DNA2-AuNPs. The ECL emission of PTCA/NH_2MIL-125 was quenched by Au NPs because of the spectral overlap between PTCA and Au NPs. With MC-LR being included, the aptamer separated from the sensor, breaking the bridge between PTCA/NH_2MIL-125 and Au NPs, and the ECL emission was restored. The quantifi-

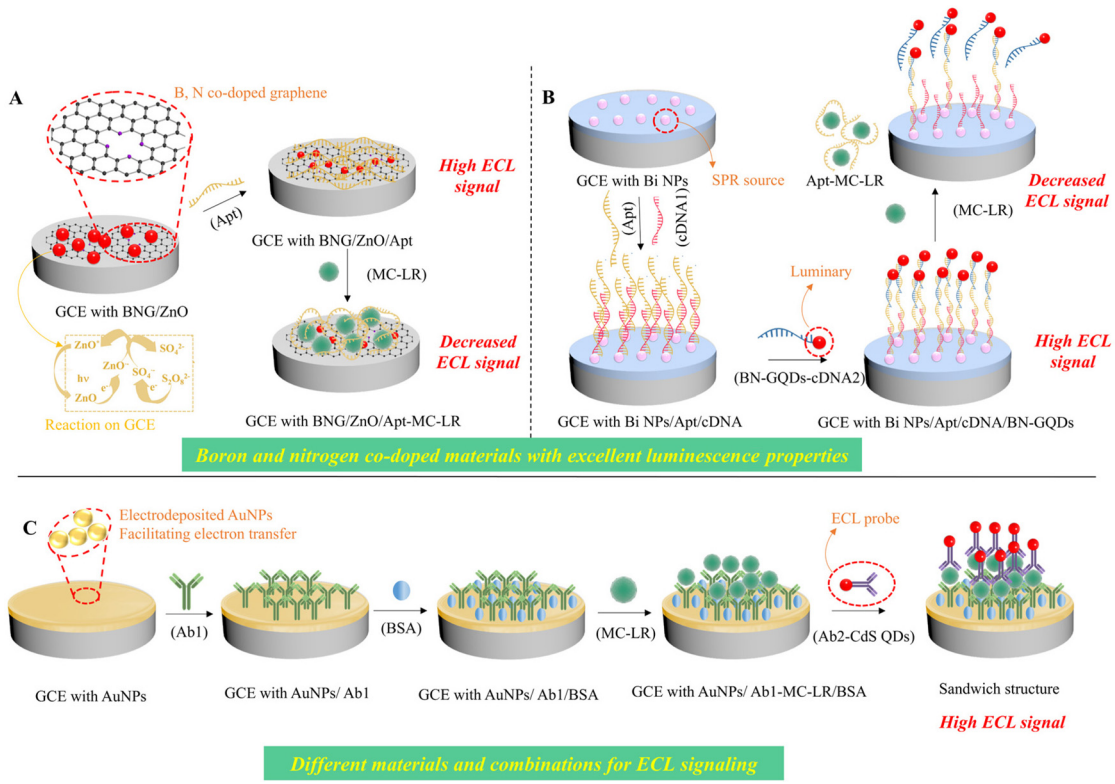

Fig. 9 (A) Schematic overview of the development and detection mechanism of the ECL sensing system incorporating BNG/ZnO.[108] (B) Schematic portrayal of the fabrication and sensing mechanism of a Bi NP and BN-GQD-based sensor for MC-LR detection *via* SPR.[109] (C) ECL immunodetection system leveraging CdS QDs for MC-LR.[111]

cation of MC-LR was accomplished by tracking the elevation in the ECL signal following MC-LR binding, with a sensitivity range spanning from 9.95 pg L^{-1} to 99.5 μg L^{-1} and a LOD of 3.58 pg L^{-1}.[114]

ECL signal transduction is highly effective for detecting MC-LR due to its high sensitivity, low background signal, broad linear range and quick response time, which is ideal for detecting low levels of MC-LR. Nevertheless, issues such as the

Table 2 Comparison of analytical performance of representative optical-based sensors for the detection of MC-LR

Method of detection	Recognition elements	Nanoparticle/composite used	Linear range (μg L^{-1})	LOD (μg L^{-1})	Sample type	Ref.
Colorimetry	Ab	G4-AuNPs conjugates	0.1–10	0.05	Lake water	69
	Apt	AuNPs	0.5–75 000	0.37	Tap/pond water	70
	Apt	Au NPs dimers	0.1–250	0.05	River water, PBS buffer and human serum	71
	mAb	PDA vesicles	1–100	1.0	—	72
	mAb and Apt	PDA/CuNPs	0.05–25	0.05	Drinking/river water, orange juice and milk	73
	Apt	GO hydrogel	0.65–1000	0.217	Tap water and serum	74
	Apt	Cu/Au/Pt TNs-encapsulated DNA hydrogel	0.004–10	0.003	Tap and drinking water	75
Fluorescence	mAb	CdSe/ZnS QDs/Cy5.5 dye	0.10–4.0	0.03	Water	78
	Apt	MB-QD525/PoPo3 dye	0.0001–100	10^{-4}	Cyanobacterial culture and river water	79
	Apt	MoS_2 QDs and Au NPs	0.05–40	0.01	Reservoir water	80
	pAb	Si-CDs/ABTS/H_2O_2/HRP	0.001–3.20	6×10^{-4}	Tap/lake/drinking water and crucian	33
	Coordination of Fe^{3+}	N/P CDs	0.05–3	0.017	Tap/sea water	81
	MIP	MIP@CQDs@SiO_2	1–1000	9.3×10^{-3}	Lake/tap water	59
	mAb	Colloidal graphene	0–500	0.93	Lake/tap water and PBST buffer	82
	Apt	SWNTs and dapoxyl	0.4–1200	0.137	Tap water and serum	83
	Ab	Au nano-crosses/Cy5	0.02–16	0.007	Fish	84
	Apt	GNSs/Cy3	0.1 to 50	0.50	Tap/lake/river water	85
	Apt	Au NPs/FAM/DNase I enzyme	0.25–20	0.83	Tap water	86
	Apt	CRISPR/Cas12a/FAM	1×10^{-5}–10	3.02×10^{-6}	River water	87
	Apt	CRISPR/Cas14a/FAM/2D-pMOFs	0.05–1000	0.019	Tap/drinking water	88
SERS	Apt	Au NF-Ag NP	0.01–10	8.6×10^{-3}	Lake water	92
	Apt	MNPs/AuNPs	0.01–200	0.002	Tap water	120
	Apt	Au@gap@AgAu NPs and GO/Fe_3O_4 NPs	0.01–100	9.82×10^{-3}	Lake water	94
	Apt	Au@label@Ag@Au NPs	10–100	8×10^{-4}	*M. aeruginosa* culture	95
	mAb	GNS@Raman reporter@SiO_2	0.01–100	0.014	Tap water and *M. aeruginosa* culture	96
	Apt	HTNP AgClAu : p-GO	0.01–5.0	6.3×10^{-3}	Reservoir water	97
	Apt	AuNPs/GO composite	SERS for qualitative detection FET for quantitative detection		Deionized/tap/fresh lake water	98
SPR	mAb	Self-assembled monolayer	0.2–2.0	0.073	Drinking water	101
	mAb	CM5 chip	0.69–4.24	0.005	Cyanobacterial cultures	102
	mAb	SAMs on the SPR chip	0.013–1.01	0.0039	Lake water	103
ECL	Apt	BN-GHs	10^{-4}–1.0	3.0×10^{-5}	Tap/contaminated water and human serum	107
	Apt	BNG/ZnO	10^{-4}–5.0	3.0×10^{-5}	Tap/lake water	108
	Apt	BN-GQDs and Bi NPs	3.0×10^{-5}–5.0	3.0×10^{-6}	Tap/lake water	109
	mAb	CdS QDs.	0.01–50	0.0028	River water	111
	Apt	PTCA/NH_2MIL-125 and AuNPs	9.95×10^{-6}–99.5	3.58×10^{-6}	Tap/river water	114
LSPR	Ab	Antigen–ovalbumin modified biological magnetosomes	1–20	—	Seafood	117
CL	Nanobody	—	—	0.33	Lake water	118
	Ab	HRP-functionalized Si NPs	0.02–200	0.006	Tap/lake/bottled drinking water	119

stability of luminescent reagents, electrode contamination, and the need for rigorous sample pretreatment still need to be addressed.

3.6 Other signal transduction methods

Apart from signal transduction methods mentioned above, localized surface plasmon resonance (LSPR) techniques and chemiluminescence (CL) techniques have also been employed for the detection of MC-LR. LSPR is an optical phenomenon arising from the interaction between electromagnetic waves and the conduction electrons within metals. The localized field decay characteristic of LSPR diminishes the solution's susceptibility to interference caused by refractive index variations and enhances the sensitivity to refractive index alterations at the surface. AuNPs are frequently utilized in LSPR.[115,116] Sun and colleagues developed a simple LSPR assay utilizing antibody-functionalized gold nanorods for signal detection and biological magnetosomes modified with antigen–ovalbumin for signal amplification to detect MC-LR in seafood samples. The assay showed a linear response to MC-LR concentrations from 1 to 20 ng mL^{-1}.[117] CL techniques involve the emission of light resulting from a redox reaction, where a molecule within the reaction system absorbs energy, becomes excited, and then emits light as it returns to its ground state. The advantages of chemiluminescence techniques include high sensitivity, a wide linear detection range and rapid reaction. Zhao *et al.* developed a multivalent bifunctional nanobody-based chemiluminescent immunoassay (MBN-CLIA) for MC-LR detection in lake water, with a LOD of 0.33 ng mL^{-1}.[118] Lu *et al.* developed a swift sandwich immunoassay method for detecting MC-LR in aqueous environments, utilizing flow injection chemiluminescence. By employing Si/Ab2 as the signal probe, they achieved a 13-fold increase in the CL signal intensity, which resulted in a wide quantification range spanning from 0.02 to 200 μg L^{-1} and a sensitive LOD of 6 ng L^{-1}.[119]

Based on the aforementioned discussion, various optical strategies including colorimetry, fluorescence, SERS, SPR, ECL signalling and other signal transduction methods have been successfully employed for detecting MC-LR. The performance characteristics of these optical sensors for detecting MC-LR are summarized in Table 2.

4. Conclusion and future prospects

It is widely recognized that strengthening the surveillance of MC-LR is essential for safeguarding environmental safety and public health, given its detrimental impact on ecosystems. Optical sensors offer a straightforward, rapid and economical technique for the sensitive and reliable detection of MC-LR. Consequently, this review systematically delineates recent advances in optical sensors for the sensitive and reliable detection of MC-LR, providing a comprehensive summary of the recognition elements and optical signal transduction mechanisms utilized.

The selection of suitable recognition receptors is a critical determinant of sensor performance. Initially, protein phosphatases were introduced as recognition receptors in sensors for MC-LR, but their poor specificity led to their gradual replacement by other recognition elements. Recently, the microcystin degradation enzyme, MlrB, has emerged as a promising recognition element with potential applicability. However, it requires further investigation. pAbs, mAbs, antibody fragments, and AV_{HH}-MV_H exhibit high affinity for MC-LR, with IC_{50} values as low as 0.06 μg L^{-1}, and are widely employed in MC-LR sensor construction. Nevertheless, these antibodies exhibit considerable cross-reactivity with MC variants, particularly MC-RR and MC-YR. MIPs offer unparalleled advantages over other biomolecules in terms of chemical, mechanical, and storage stability. The selection of appropriate functional monomers and polymerization methods is crucial for fabricating high-affinity MIPs with MC-LR-specific cavities. Aptamers have demonstrated considerable advancement in serving as recognition elements in biosensors, attributed to their specificity and strong binding affinity. A high-affinity aptamer for MC-LR, with a K_d value of 50 nM, has been selected and widely applied in sensors. However, major limitations remain before aptamers can be widely adopted, such as the impact of ionic strength, total protein concentration, and temperature on biosensing performance. Taken together, these recognition elements each exhibit distinct advantages. The selection of an appropriate signal recognition element should be based on the subsequent signal transduction approaches, sample characteristics, and detection fields. Furthermore, improving the specificity and affinity of these enzymes, pAbs, mAbs, MIPs, and aptamers through biological or chemical modifications, and developing new recognition units with superior selectivity and sensitivity toward MC-LR, should be areas of further study.

For optical signal transduction, ingeniously designed strategies have been successfully implemented for detecting MC-LR, with a specific emphasis on the colorimetric, fluorescence, SERS, SPR, and ECL sensing strategies. A range of nanomaterials, such as QDs, noble metal nanomaterials, carbon-based nanomaterials and MOFs, have been employed to transduce the recognition information into an optical signal. These optical sensors have demonstrated potential practical applications, achieving accurate quantification of MC-LR in actual water samples, and in some cases, in complex samples such as serum and tissue. However, several challenges remain. The majority of optical sensors remain in the experimental phase, concentrating on the demonstration of concept and validation. Additionally, linking recognition elements with nanomaterials for functionalization can inevitably add to the complexity, expense, and time needed for the development of optical sensors. Moreover, this conjugation might diminish the recognition elements' ability to distinguish targets effectively.

With the remarkable progress in the design of optical sensors for MC-LR detection, tremendous opportunities and attractive application prospects are emerging. The following

aspects are worth paying attention: (1) although the MC-LR exhibits the highest toxicity among MCs, other harmful cyanotoxins are also present in most of the water resources and also require attention. Therefore, the development of optical sensors with multi-target detection capabilities, combined with high-throughput detection tools such as microfluidics, is recommended for simultaneous detection of MC-LR and other cyanotoxins. (2) Owing to the simplicity of optical sensing, integrating field-deployable devices holds promise for on-site applications. Leveraging compact devices and wireless connectivity, the binding event of MC-LR can be transformed into a quantifiable digital signal using portable devices like smartphones, with the analysis results being sent to remote servers. This method enables field detection, moving beyond the confines of a laboratory setting, and heralds the advent of a new class of analytical tools for real-time surveillance. (3) Benefiting from the appreciable sensitivity of the optical sensors, a suitable prediction system for the early determination of MC-LR at picogram levels during cyanobacteria bloom could be constructed based on the integration of optical sensing with multi-disciplinary technologies, which could significantly enhance environment safety and human health protection.

Author contributions

Heng Dai: conceptualization, literature search, and writing – original draft. Jun Liu: conceptualization and writing – original draft. Shanlin Wang: validation. Bin Wang: visualization. Tianhan Kai: supervision and methodology. Pian Wu: supervision, project administration, funding acquisition, and writing – review & editing. Ping Ding: supervision, project administration, and funding acquisition.

Data availability

No primary research results, software or code have been included and no new data were generated or analysed as part of this review.

Conflicts of interest

There are no conflicts of interest to declare.

Acknowledgements

This work was supported by the National Natural Science Foundation of China (grant number 82373635), the Natural Science Foundation of Hunan (grant number 2025JJ60624), the Natural Science Foundation of Changsha (grant number kq2402240), the Start-up Funds from Central South University (grant number 502044013), the School enterprise cooperation program of Central South University (grant number 2023XQLH053) and the Graduate Research Innovation Program of Central South University (grant number: 2025ZZTS0901).

References

1 R. I. Woolway, B. M. Kraemer, J. D. Lenters, C. J. Merchant, C. M. O'Reilly and S. Sharma, *Nat. Rev. Earth Environ.*, 2020, **1**, 388–403.
2 E. M. L. Janssen, *Water Res.*, 2019, **151**, 488–499.
3 X. Y. Ren, M. Y. Mao, M. Q. Feng, T. J. Peng, X. Z. Long and F. Yang, *Water Res.*, 2024, **251**, 13.
4 Y. L. Shu, H. Wang, H. L. Jiang, S. W. Zhou, L. Y. Zhang, Z. F. Ding, P. Hong, J. He and H. L. Wu, *Environ. Pollut.*, 2024, **345**, 9.
5 H. Mashayekhi-sardoo, R. Rezaee, B. Riahi-Zanjani and G. Karimi, *Toxicon*, 2024, **243**, 15.
6 G. H. Xu, Y. Luo, D. H. Xu, Y. H. Ma, Y. B. Chen and X. D. Han, *Toxicon*, 2022, **210**, 78–88.
7 S. Y. Zhang, X. D. Du, H. H. Liu, M. D. Losiewic, X. H. Chen, Y. Ma, R. Wang, Z. H. Tian, L. J. Shi, H. X. Guo and H. Z. Zhang, *Environ. Res.*, 2021, **192**, 17.
8 L. H. Cao, I. Y. Massey, H. Feng and F. Yang, *Toxins*, 2019, **11**, 20.
9 M. M. Abdel-Daim, A. A. Sayed, A. Abdeen, L. Aleya, D. Ali, A. A. Alkahtane, S. Alarifi and S. Alkahtani, *Oxid. Med. Cell. Longevity*, 2019, **2019**, 10.
10 M. Alosman, L. H. Cao, I. Y. Massey and F. Yang, *Toxin Rev.*, 2021, **40**, 517–526.
11 K. F. Ge, X. D. Du, H. H. Liu, R. Y. Meng, C. R. Wu, Z. X. Zhang, X. Liang, J. Yang and H. Z. Zhang, *Arch. Toxicol.*, 2024, **98**, 663–687.
12 C. Pan, L. Zhang, X. N. Meng, H. X. Qin, Z. Xiang, W. Y. Gong, W. X. Luo, D. M. Li and X. D. Han, *Chemosphere*, 2021, **263**, 15.
13 S. Gu, M. X. M. Jiang and B. Zhang, *Toxins*, 2022, **14**, 11.
14 W. H. Organization, *Cyanobacterial toxins: microcystins*, World Health Organization, 2020.
15 I. Y. Massey, P. Wu, J. Wei, J. Y. Luo, P. Ding, H. Y. Wei and F. Yang, *Toxins*, 2020, **12**, 32.
16 H. X. Zhang, B. Y. Li, Y. P. Liu, H. Y. Chuan, Y. Liu and P. Xie, *J. Hazard. Mater.*, 2022, **424**, 24.
17 H. K. Kordasht, S. Hassanpour, B. Baradaran, R. Nosrati, M. Hashemzaei, A. Mokhtarzadeh and M. de la Guardia, *Biosens. Bioelectron.*, 2020, **165**, 12.
18 B. Z. Li, Q. S. Wang, M. Sohail, X. Zhang, H. He and L. Lin, *Microchem. J.*, 2023, **189**, 11.
19 A. Uniyal, G. Srivastava, A. Pal, S. Taya and A. Muduli, *Plasmonics*, 2023, **18**, 735–750.
20 T. Y. Suo, M. Sohail, S. Y. Xie, B. Z. Li, Y. Chen, L. H. Zhang and X. Zhang, *J. Hazard. Mater.*, 2021, **403**, 13.
21 V. Vogiazi, A. de la Cruz, S. Mishra, V. Shanov, W. R. Heineman and D. D. Dionysiou, *ACS Sens.*, 2019, **4**, 1151–1173.

22 Y. García, M. Vera, J. D. Giraldo, K. Garrido-Miranda, V. A. Jiménez, B. F. Urbano and E. D. Pereira, *Anal. Chem.*, 2022, **94**, 464–478.
23 P. F. Pang, Y. Q. Lai, Y. L. Zhang, H. B. Wang, X. A. Conlan, C. J. Barrow and W. R. Yang, *Bull. Chem. Soc. Jpn.*, 2020, **93**, 637–646.
24 A. Miglione, M. Napoletano and S. Cinti, *Biosensors*, 2021, **11**, 16.
25 Y. Kim, Y. Jeon, M. Na, S. J. Hwang and Y. Yoon, *Sensors*, 2024, **24**, 18.
26 A. Sassolas, G. Catanante, D. Fournier and J. L. Marty, *Talanta*, 2011, **85**, 2498–2503.
27 G. Catanante, L. Espin and J.-L. Marty, *Biosens. Bioelectron.*, 2015, **67**, 700–707.
28 Y. Li, S. Si, F. Huang, J. Wei, S. Dong, F. Yang, H. Li and S. Liu, *Bioelectrochemistry*, 2022, **144**, 108000.
29 B.-H. Liu, F.-Y. Yu and F. S. Chu, *J. Agric. Food Chem.*, 1996, **44**, 4037–4042.
30 J. S. Metcalf, S. G. Bell and G. A. Codd, *Water Res.*, 2000, **34**, 2761–2769.
31 L. Ruiyi, X. Qianfang, L. Zaijun, S. Xiulan and L. Junkang, *Biosens. Bioelectron.*, 2013, **44**, 235–240.
32 X. Sun, H. Shi, H. Wang, L. Xiao and L. Li, *Anal. Lett.*, 2010, **43**, 533–544.
33 Z.-L. Xu, S.-L. Ye, L. Luo, X. Hua, J.-X. Lai, X.-P. Cai, Q.-W. Liang, H.-T. Lei, Y.-M. Sun, Y.-P. Chen and X. Shen, *Sci. Total Environ.*, 2020, **708**, 134614.
34 S. Nagata, H. Soutome, T. Tsutsumi, A. Hasegawa, M. Sekijima, M. Sugamata, K.-I. Harada, M. Suganuma and Y. Ueno, *Nat. Toxins*, 1995, **3**, 78–86.
35 A. Zeck, M. G. Weller, D. Bursill and R. Niessner, *Analyst*, 2001, **126**, 2002–2007.
36 R. Al-Ammar, A. Nabok, A. Hashim and T. Smith, *J. Phys.: Conf. Ser.*, 2013, **450**, 012006.
37 S. Herranz, M. D. Marazuela and M. C. Moreno-Bondi, *Biosens. Bioelectron.*, 2012, **33**, 50–55.
38 L. Q. Liu, C. R. Xing, H. J. Yan, H. Kuang and C. L. Xu, *Sensors*, 2014, **14**, 14672–14685.
39 J.-W. Sheng, M. He and H.-C. Shi, *Anal. Chim. Acta*, 2007, **603**, 111–118.
40 H.-C. Shi, B.-D. Song, F. Long, X.-H. Zhou, M. He, Q. Lv and H.-Y. Yang, *Environ. Sci. Technol.*, 2013, **47**, 4434–4441.
41 J. Tian, H. Zhao, X. Quan, Y. Zhang, H. Yu and S. Chen, *Sens. Actuators, B*, 2014, **196**, 532–538.
42 Z. Xiao-hong, S. Bao-dong, S. Han-chang, L. Lan-hua, G. Hong-li and H. Miao, *Sens. Actuators, B*, 2014, **198**, 150–156.
43 A. Zeck, A. Eikenberg, M. G. Weller and R. Niessner, *Anal. Chim. Acta*, 2001, **441**, 1–13.
44 C. Murphy, E. Stack, S. Krivelo, D. A. McPartlin, B. Byrne, C. Greef, M. J. Lochhead, G. Husar, S. Devlin, C. T. Elliott and R. J. O'Kennedy, *Biosens. Bioelectron.*, 2015, **67**, 708–714.
45 C. X. Xu, X. Q. Liu, Y. Liu, X. Zhang, C. Z. Zhang, J. H. Li and X. J. Liu, *Talanta*, 2019, **197**, 397–405.
46 W. A. Hassanain, E. L. Izake, M. S. Schmidt and G. A. Ayoko, *Biosens. Bioelectron.*, 2017, **91**, 664–672.
47 L. Zhang, H. Dong, H. Li, B. Li, G. Zhao, H. Cai, L. Chen and J. Dong, *Microchem. J.*, 2021, **167**, 106295.
48 M. Pírez-Schirmer, M. Rossotti, N. Badagian, C. Leizagoyen, B. M. Brena and G. González-Sapienza, *Anal. Chem.*, 2017, **89**, 6800–6806.
49 C. Xu, D. He, Y. Zu, S. Hong, J. Hao and J. Li, *J. Hazard. Mater.*, 2021, **406**, 124596.
50 P. Fernando, M. W. Glasscott, K. Pokrzywinski, B. M. Fernando, G. K. Kosgei and L. C. Moores, *Crit. Rev. Anal. Chem.*, 2022, **52**, 1244–1258.
51 I. Chianella, M. Lotierzo, S. A. Piletsky, I. E. Tothill, B. Chen, K. Karim and A. P. F. Turner, *Anal. Chem.*, 2002, **74**, 1288–1293.
52 R. J. Zhao, J. Li, C. S. Wu, J. Cai, S. Q. Li, A. F. Li and L. Zhong, *Water Sci. Technol.*, 2023, **88**, 572–585.
53 R. B. Queirós, J. P. Noronha, P. V. S. Marques, J. S. Fernandes and M. G. F. Sales, *Analyst*, 2012, **137**, 2437–2444.
54 R. B. Queirós, S. O. Silva, J. P. Noronha, O. Frazão, P. Jorge, G. Aguilar, P. V. S. Marques and M. G. F. Sales, *Biosens. Bioelectron.*, 2011, **26**, 3932–3937.
55 S.-D. Pan, X.-H. Chen, X.-P. Li, M.-Q. Cai, H.-Y. Shen, Y.-G. Zhao and M.-C. Jin, *J. Mater. Chem. A*, 2015, **3**, 23042–23052.
56 J. Chen, P. Gao, H. Wang, L. Han, Y. Zhang, P. Wang and N. Jia, *J. Mater. Chem. C*, 2018, **6**, 3937–3944.
57 R. B. Queirós, J. P. Noronha, P. V. S. Marques and M. G. F. Sales, *Procedia Eng.*, 2012, **47**, 758–761.
58 Z. Wu, D. He, B. Cui and Z. Jin, *Food Chem.*, 2019, **283**, 517–521.
59 Z. Qi, R. Lu, S. Wang, C. Xiang, C. Xie, M. Zheng, X. Tian and X. Xu, *Microchem. J.*, 2021, **161**, 105798.
60 M. L. Song, H. H. Sun, J. Yu, Y. Wang, M. F. Li, M. C. Liu and G. H. Zhao, *ACS Appl. Mater. Interfaces*, 2021, **13**, 37212–37222.
61 M. Liu, X. Ding, Q. Yang, Y. Wang, G. Zhao and N. Yang, *J. Hazard. Mater.*, 2017, **331**, 309–320.
62 H. B. Bostan, S. M. Taghdisi, J. L. Bowen, N. Demertzis, R. Rezaee, Y. Panahi, A. M. Tsatsakis and G. Karimi, *Biosens. Bioelectron.*, 2018, **119**, 110–118.
63 C. Nakamura, T. Kobayashi, M. Miyake, M. Shirai and J. Miyakea, *Mol. Cryst. Liq. Cryst. Sci. Technol., Sect. A*, 2001, **371**, 369–374.
64 K.-D. Gu and M. Famulok, *Zhonghua Yufang Yixue Zazhi*, 2004, **38**, 369–373.
65 A. Ng, R. Chinnappan, S. Eissa, H. Liu, C. Tlili and M. Zourob, *Environ. Sci. Technol.*, 2012, **46**, 10697–10703.
66 S. M. Nokandeh, R. Eivazzadeh-Keihan, M. S. Bani, I. Zare, H. M. Kang, M. T. Yaraki, M. Mahdavi, A. Maleki and R. S. Varma, *Coord. Chem. Rev.*, 2025, **522**, 22.
67 Y. P. Liu, B. Y. Li, H. X. Zhang, Y. Liu and P. Xie, *Coord. Chem. Rev.*, 2022, **457**, 30.
68 J. W. Sun, Y. X. Lu, L. Y. He, J. W. Pang, F. Y. Yang and Y. Y. Liu, *TrAC, Trends Anal. Chem.*, 2020, **122**, 20.

69 Y. Zhu, L. Xu, W. Ma, W. Chen, W. Yan, H. Kuang, L. Wang and C. Xu, *Biosens. Bioelectron.*, 2011, **26**, 4393–4398.
70 X. Li, R. Cheng, H. Shi, B. Tang, H. Xiao and G. Zhao, *J. Hazard. Mater.*, 2016, **304**, 474–480.
71 F. Wang, S. Liu, M. Lin, X. Chen, S. Lin, X. Du, H. Li, H. Ye, B. Qiu, Z. Lin, L. Guo and G. Chen, *Biosens. Bioelectron.*, 2015, **68**, 475–480.
72 Y. Xia, J. Deng and L. Jiang, *Sens. Actuators, B*, 2010, **145**, 713–719.
73 X. Tang, Z. Yin, X. Lei, Y. Zeng, Z. Zhang, Y. Lu, G. Zhou, L. Li and X. Wu, *Nanomaterials*, 2019, **9**, 332.
74 K. Abnous, N. M. Danesh, M. Ramezani and S. M. Taghdisi, *Microchim. Acta*, 2017, **184**, 4451–4457.
75 P. Wu, S. Li, X. S. Ye, B. A. Ning, J. L. Bai, Y. Peng, L. Li, T. Han, H. Y. Zhou, Z. X. Gao and P. Ding, *Anal. Chim. Acta*, 2020, **1134**, 96–105.
76 Y. H. Shin, M. T. Gutierrez-Wing and J. W. Choi, *J. Electrochem. Soc.*, 2021, **168**, 17.
77 M. Y. Chen, Z. Q. Ning, X. Ge, E. R. Yang, Q. Sun, F. Yin, M. M. Zhang, Y. J. Zhang and Y. F. Shen, *Biosens. Bioelectron.*, 2023, **219**, 8.
78 L. Feng, A. Zhu, H. Wang and H. Shi, *Biosens. Bioelectron.*, 2014, **53**, 1–4.
79 E.-H. Lee and A. Son, *Chem. Eng. J.*, 2019, **359**, 1493–1501.
80 H. Cao, W. Dong, T. Wang, W. Shi, C. Fu and Y. Wu, *ACS Sustainable Chem. Eng.*, 2020, **8**, 10939–10946.
81 X. Wang, J. Yu, W. Ji, M. Arabi, L. Fu, B. Li and L. Chen, *ACS Appl. Nano Mater.*, 2021, **4**, 6852–6860.
82 M. Liu, H. Zhao, S. Chen, H. Yu and X. Quan, *Environ. Sci. Technol.*, 2012, **46**, 12567–12574.
83 S. M. Taghdisi, N. M. Danesh, M. Ramezani, N. Ghows, S. A. Mousavi Shaegh and K. Abnous, *Talanta*, 2017, **166**, 187–192.
84 Y. Li, J. Sun, L. Wu, J. Ji, X. Sun and Y. Qian, *Biosens. Bioelectron.*, 2014, **62**, 255–260.
85 M. Li, H. Lin, S. K. Paidi, N. Mesyngier, S. Preheim and I. Barman, *ACS Sens.*, 2020, **5**, 1419–1426.
86 W. Xie, S. He, S. Fang, L. Liang, B. Shi and D. Wang, *Anal. Chim. Acta*, 2021, **1173**, 338698.
87 Y. Kang, G. Su, Y. Yu, J. Cao, J. Wang and B. Yan, *Environ. Sci. Technol.*, 2022, **56**, 4101–4110.
88 P. Wu, X. Ye, D. Wang, F. Gong, X. Wei, S. Xiang, J. Zhang, T. Kai and P. Ding, *J. Hazard. Mater.*, 2022, **424**, 127690.
89 T. Itoh, M. Prochazka, Z. C. Dong, W. Ji, Y. S. Yamamoto, Y. Zhang and Y. Ozaki, *Chem. Rev.*, 2023, **123**, 1552–1634.
90 L. L. Yang, Y. S. Peng, Y. Yang, J. J. Liu, H. L. Huang, B. H. Yu, J. M. Zhao, Y. L. Lu, Z. R. Huang, Z. Y. Li and J. R. Lombardi, *Adv. Sci.*, 2019, **6**, 13.
91 H. Y. Chen, C. Y. Xi, H. B. Xu, M. J. Ye, Y. He, B. B. Chen and D. W. Li, *ACS Appl. Mater. Interfaces*, 2024, **16**, 67134–67154.
92 Y. Zhao, X. Yang, H. Li, Y. Luo, R. Yu, L. Zhang, Y. Yang and Q. Song, *Chem. Commun.*, 2015, **51**, 16908–16911.
93 W. Yue, B. Y. Lin, Y. Y. Huang, Y. L. Wang, Y. Y. Yao, L. F. Chen, Y. B. Zeng, L. Li, Z. S. Qian and L. H. Guo, *Sens. Actuators, B*, 2023, **380**, 6.
94 Y. Zhao, F. Zheng, W. Ke, W. Zhang, L. Shi and H. Liu, *Anal. Chem.*, 2019, **91**, 7162–7172.
95 X. Luo, X. Zhao, G. Q. Wallace, M.-H. Brunet, K. J. Wilkinson, P. Wu, C. Cai, C. G. Bazuin and J.-F. Masson, *ACS Appl. Mater. Interfaces*, 2021, **13**, 6545–6556.
96 M. Li, S. K. Paidi, E. Sakowski, S. Preheim and I. Barman, *ACS Sens.*, 2019, **4**, 1203–1210.
97 L. Ma, X. Zhao, Z. Zhang, H. Ge and J. Wang, *Talanta*, 2022, **236**, 122864.
98 M. Tian, J. Wang, C. Li, Z. Wang, G. Liu, E. Lv, X. Zhao, Z. Li, D. Cao, H. Liu, C. Zhang, S. Xu and B. Man, *Biosens. Bioelectron.*, 2022, **212**, 114434.
99 T. M. S. Ashrafi and G. Mohanty, *Plasmonics*, 2025, DOI: **10.1007/s11468-024-02740-4**.
100 H. Liu, Y. S. Fu, R. Z. Yang, J. C. Guo and J. H. Guo, *Analyst*, 2023, **148**, 6146–6160.
101 S. Herranz, M. Bocková, M. D. Marazuela, J. Homola and M. C. Moreno-Bondi, *Anal. Bioanal. Chem.*, 2010, **398**, 2625–2634.
102 S. Devlin, J. P. Meneely, B. Greer, K. Campbell, V. Vasconcelos and C. T. Elliott, *Talanta*, 2014, **122**, 8–15.
103 J. S. Tan, Z. R. Dai, K. M. Zhou, L. Zhang, M. He, Y. D. Tan and X. H. Zhou, *Environ. Sci. Technol.*, 2023, **57**, 8313–8322.
104 W. Ussler III, G. J. Doucette, C. M. Preston, C. Weinstock, N. Allaf, B. Roman, S. Jensen, K. Yamahara, L. A. Lingerfelt, C. M. Mikulski, B. W. Hobson, B. Kieft, B. Raanan, Y. W. Zhang, R. M. Errera, S. A. Ruberg, P. A. Den Uyl, K. D. Goodwin, S. D. Soelberg, C. E. Furlong, J. M. Birch and C. A. Scholin, *Limnol. Oceanogr.:Methods*, 2024, **22**, 681–699.
105 W. Lv, H. Ye, Z. Yuan, X. Liu, X. Chen and W. Yang, *TrAC, Trends Anal. Chem.*, 2020, **123**, 115767.
106 J. Mehta, N. Dilbaghi, N. K. Singhal, G. Marrazza, A. Kaushik and S. Kumar, *Chem. Eng. J.*, 2023, **477**, 30.
107 X. Du, D. Jiang, N. Hao, J. Qian, L. Dai, L. Zhou, J. Hu and K. Wang, *Anal. Chem.*, 2016, **88**, 9622–9629.
108 R. Yuan, L. Ding, F. You, Z. Wen, Q. Liu and K. Wang, *Sens. Actuators, B*, 2021, **349**, 130795.
109 R. Yuan, Q. Liu, H. Hong, H. Ma, L. Xiao, Y. Li, D. Jiang, N. Hao and K. Wang, *J. Hazard. Mater.*, 2022, **434**, 128877.
110 E. R. Yang, H. Yang, Z. Q. Ning, Y. F. Fang, M. Y. Chen, Y. J. Zheng, W. H. Xu, G. Q. Wu, Y. J. Zhang and Y. F. Shen, *Anal. Chem.*, 2022, **94**, 16510–16518.
111 J.-J. Zhang, T.-F. Kang, Y.-C. Hao, L.-P. Lu and S.-Y. Cheng, *Sens. Actuators, B*, 2015, **214**, 117–123.
112 Q. Sun, Z. Q. Ning, E. R. Yang, F. Yin, G. Q. Wu, Y. J. Zhang and Y. F. Shen, *Angew. Chem., Int. Ed.*, 2023, **62**, 8.
113 F. Yin, E. R. Yang, X. Ge, Q. Sun, F. Mo, G. Q. Wu and Y. F. Shen, *Chin. Chem. Lett.*, 2024, **35**, 6.
114 J. Li, D. Jiang, X. Shan, W. Wang and Z. Chen, *Microchim. Acta*, 2020, **187**, 474.

115 G. S. Geleta, *Anal. Bioanal. Chem.*, 2022, **414**, 7103–7122.
116 C. Y. Zheng, M. M. Yin, B. Y. Su, A. H. Peng, Z. Y. Guo, X. M. Chen and X. Chen, *Talanta*, 2021, **221**, 8.
117 X. L. Sun, L. Y. Wu, J. Ji, D. L. Jiang, Y. Z. Zhang, Z. J. Li, G. Y. Zhang and H. X. Zhang, *Biosens. Bioelectron.*, 2013, **47**, 318–323.
118 D. Y. Zhao, M. Hu, C. H. Hu, D. Wang, H. L. Chen, Y. W. Ou, R. L. Liu, X. Y. Li, L. Wu, P. Liu, Z. W. Shen and Q. Chen, *Talanta*, 2025, **283**, 7.
119 J. S. Lu, W. Wei, L. H. Yin, Y. P. Pu and S. Q. Liu, *Analyst*, 2013, **138**, 1483–1489.
120 D. Y. He, Z. Z. Wu, B. Cui and Z. Y. Jin, *Food Chem.*, 2019, **278**, 197–202.